Eur. Phys. J. AP **3**, 321–342 (1998)

THE EUROPEAN PHYSICAL JOURNAL APPLIED PHYSICS

Unsteady flow in cone and plate geometry: how computation can help rheometry

J. Passard[1,a], R. Kouitat Njiwa[2], and P. Perré[3]

[1] Université Henri Poincaré, Laboratoire d'Énergétique et de Mécanique (LEMTA), IUT Nancy Brabois, dept. Génie Civil, 54601 Villers-lès-Nancy Cedex, France
[2] Laboratoire de Sciences et Génie des Surfaces (LSGS), École des mines, Parc de Saurupt, 54042 Nancy Cedex, France
[3] Laboratoire des Sciences Forestières, École Nationale du Génie Rural des Eaux et Forêt (ENGREF), 14 rue Girardet, 54042 Nancy Cedex, France

Received: 12 November 1997 / Revised: 26 May 1998 / Accepted: 2 June 1998

Abstract. The use of rheometers for the evaluation of rheological properties and the establishment of behaviour laws for fluids requires the knowledge of the shear rate at any moment and everywhere in the region between the cone and the plate, referred to as "the gap" throughout this paper. However, the accurate determination of the shear rate supposes that the constitutive equation of the fluid is known beforehand. In order to avoid this paradox, rheometers are generally built such that the shear rate is supposed to be approximately constant throughout the gap. This approximation is realistic for steady flow but may be crude for other types of fluid motion. The aim of the present work is to determine the limits of validity of such an approximation when testing complex fluids in a cone and plate geometry. In this paper, only purely viscous properties are taken into account. The numerical solution is based on the control-volume method. When non-linear and time-dependent effects occur, it is shown that the flow cannot be represented by simple shearing conical surfaces. This result is especially important for the characterisation of time-dependent fluids (as thixotropic fluids), typical of unsteady flow. Finally the abilities of the proposed model which is named "RHEOUTIL" are highlighted by comparison between numerical simulations and experimental results. The analysis of non Newtonian fluids emphasises the limits of the code "RHEOUTIL". Indeed, the model has to evolve in order to take into account the whole complexity of the fluid, which may also exhibit viscoelastic properties, yield stress and so on.

PACS. 47.50.+d Non Newtonian fluid flows – 83.50.By Transient deformation and flow; time-dependent properties: start-up, stress relaxation, creep, recovery, etc. – 83.85.Cg Rheological measurements

Nomenclature

$\mathcal{D}$	strain-rate tensor [s^{-1}]
$\mathcal{D}_I$	1st principal invariant of the tensor $\mathcal{D}$ [s^{-1}]
$\mathcal{D}_{II}$	2nd principal invariant of the tensor $\mathcal{D}$ [s^{-2}]
$\mathcal{D}_{III}$	3rd principal invariant of the tensor $\mathcal{D}$ [s^{-3}]
$\mathbf{I}$	unit tensor
I	system inertia [N m s^2]
J	damping coefficient [N m s]
k	torsion constant [N m rd^{-1}]
L	radius of the free liquid surface [m]
M_v	torque [N m]
$\mathbf{n}$	normal unit vector
N	frequency [Hz]
N_o	free oscillation frequency [Hz]
p	hydrostatic pressure [Pa]
P_{ij}	node of the control volume ij
R	cone radius [m]
r	space variable in sperical co-ordinates [m]
r^*	dimensionless radius variable
t	time variable [s]
t^*	dimensionless time variable
T	oscillation period [s]
$\Im$	deviatoric stress tensor [Pa]
$\mathbf{U}$	velocity vector of flow [m s^{-1}]
U_r	r component of velocity [m s^{-1}]
U_θ	θ component of velocity [m s^{-1}]
U_φ	φ component of velocity [m s^{-1}]
u	φ component of velocity [m s^{-1}]
V_{ij}	control volume ij [m^3]

Greek symbols

α	twist angle [rd]
$\dot{\gamma}$	mean shear rate [s^{-1}]
$\dot{\varepsilon}$	component of strain-rate tensor [s^{-1}]
θ	angular variable in the gap [degree]
θ_0	cone angle [degree]

[a] e-mail: joelle.passard@iutnb.u-nancy.fr

λ structural parameter
μ apparent viscosity of fluid [Pa s]
$\prod$ stress tensor [Pa]
ρ density of fluid [kg m^{-3}]
τ mean diffusion time
φ revolution angle of cone [degree]
ψ θ complementary angle [degree]
ψ_0 Cone angle [degree]
ω angular velocity of cone [rd s^{-1}]

1 Introduction

The shear flow produced between a cone and a plate is among the most-used process in rheometry, even though the shear rate field within the flow is often unknown. Kouitat *et al.* [1,2] proposed a theoretical and numerical analysis of the flow establishment in a coaxial cylinder geometry. The study presented here extends this work and proposes modeling the start-up motion in a cone and plate geometry, for different purely viscous fluids. Describing the velocity field of complex fluids is a large subject of interest which has been analyzed by several authors such as Denn and Porteous [3], Okeson and Emery [4], Crawley *et al.* [5], Burdette [6], Lee and Fuller [7]. In those different papers, the authors analyse the influence of viscoelastic properties on the transient flow in case of different kind of geometry.

Usually, the analysis of the flow does not take into account the free surface deformation, nor the inertia effect as well as the centrifugal forces responsible for the secondary flow. This simplified description of flow, called the "primary flow", assumes shearing of conical surfaces together with steady state. In that case the shear rate is supposed to be constant throughout the gap. This assumption is restrictive. Adams and Lodge [8] show that, in the case of a cone and plate steady flow, the approximation of constant shear rate is of order two and they estimate the discrepancy of that approximation for different values of the cone angle. This is obtained by development of the function $\dot{\varepsilon}\sin^2(\theta)$ in a series about $\theta = \pi/2$. In the literature, this assumption has been used by some authors to describe non-Newtonian fluid flow. We can name Cheng [9], Oka and Takami [10] and Chaturani and Narasimman [11].

Rigorously, in such a geometry, the flow is much more complex. Indeed, a secondary motion has been reported by Cox [12], Hoppmann and Miller [13] and its importance has been studied and analyzed by Batnagar and Rathna [14], Giesekus [15], Walters and Waters [16] and Cheng [17]. Many other authors proposed further analysis of the secondary flow: Turian [18], Fewell and Hellmus [19], Heuser and Krause [20], Hou [21], Olagunju and Cook [22] and Olagunju [23]. In particular, the two last references focused on cell wise flow that arises for viscoelastic fluids. The edge effect, which is the other disturbing phenomenon in cone and plate flow, has also been considered by some authors Griffiths and Walters [24], Paddon and Walters [25], Olagunju [23,26] and Heuser and Krause [20]. In order to model these complex flows, all these authors develop analytical or numerical methods.

Analysing the literature reveals that, in the rheometric situations, the secondary flow and the free surface deformation are usually phenomena of second order. Turian [18] explains: "Normal force measurements are more sensitive to the effect of the secondary motions than is the torque value; in the former they manifest themselves as a primary effect, whereas in the latter they merely exert a secondary influence". Griffiths and Walters [24] comment about the torque measurement: "Application of the theory to rheogoniometric situations indicates that edge effects are not likely to be as significant as has been conjectured in the past. For example, the error is likely to be less than 2% for cone angles of 4°or less".

The purpose of this work is to develop a useful rheometrical tool which allows the analysis of complex flow situations and the validity of the usual rheometrical assumptions to be tested.

In order to achieve our goal, we propose a stepwise approach. Consequently, the text is organized into two main parts.

The first part presents the theoretical and numerical analysis of the flow without referring to experiment. After a discussion about the chosen assumptions, the model equations of the problem are derived and we present the numerical solution procedure which is based on the control-volume method introduced by Patankar [27]. The numerical treatment of the discretised equations allows a new code "RHEOUTIL" to be achieved. The code structure is conceived from the code "TRANSPORE". This code was written by Perré [28] and initially intended for the solution of heat, mass and momentum transfers in porous media. This numerical model uses algorithms that are able to deal with stiff differential equations as well as strongly non linear problems and has been proven to be very efficient.

Then there follows an analysis of unsteady flows, for purely viscous fluids obeying to Newtonian and Power law models and for a thixotropic fluid. For these constitutive laws, it is shown that the analysis of flow are strongly dependent on the rheology of the material under test as well as on the geometry of the device and time. In that part, in order to clarify the discussion, a dimensionless presentation is used for all the numerical results.

In the second part, we propose a comparison between numerical results and experiment. Indeed, the previous theoretical study has required the following coarse assumptions: the free surface is assumed to remain spherical and the secondary flow is neglected. Consequently, the comparison of numerical results with experiment appears essential.

The Weissenberg rheometer used for this experimental work is a controlled rotation speed device. The analysis of the experimental results highlights an important physical phenomenon called the fluid structure interaction. This phenomenon is due to the torque measurement device which is carried out *via* a torsion bar. Following a detailed discussion about that particular experimental aspect, we explain how the model has been modified in order to take into account this feature.

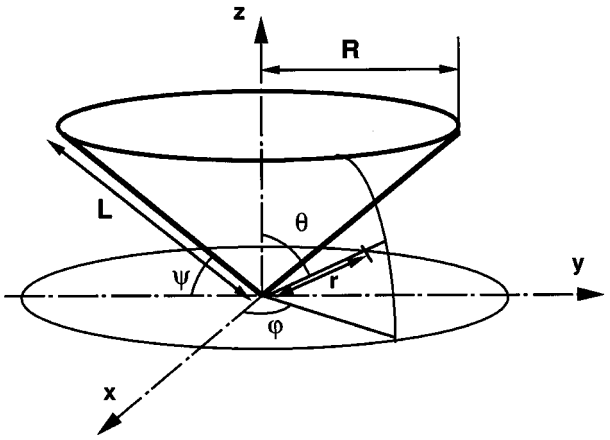

Fig. 1. Cone-plate geometry: spherical co-ordinate system.

The agreement between the simulation and the experiment for a large range of Newtonian fluids proves the abilities of the code "RHEOUTIL". Nevertheless, an analysis of the time constants reveals that the fluid structure interaction can be solved by using the lubrication assumption. After the analytical calculations, the results and the validity of the lubrication assumption are discussed. Thanks to the analytical approach, it has been possible to define criterion for analyzing the fluid structure interaction phenomena.

Analyzing what happens with non Newtonian fluids, reveals that these kind of fluids exhibit different rheological properties which can interact together. For example, a shear-thinning fluid shows also viscoelastic properties. Considering two different shear-thinning fluids, in the first case the code is in a good agreement with the experiment but the result is not as well as the Newtonian fluids ones. The second case reveals the limitation of the code because of the time dependent properties of the fluid. Therefore, it is explained in a perspective section how the code has to evolve in order to take into account this complex aspect of fluid rheology.

Considering, the code "RHEOUTIL" is developed as a tool that we hope usable by everyone, certain details are proposed in the Appendix.

2 Flow analysis and model assumptions

The geometry of interest is shown in Figure 1. Classical spherical co-ordinates (r, θ, φ) are used. R is the cone radius and one can point out that the cone is not truncated. The θ complementary angle, named ψ is introduced and its maximum value ψ_0 is of a few degrees for classical cone and plate rheometers.

In the case of the primary flow the single co-ordinate U_φ of the velocity field to be considered is:

$$U_\varphi = r \sin\theta \omega(\theta). \tag{2.1}$$

However, this velocity field does not allow the transient period to be accounted for. Indeed, the diffusion process is two dimensional in the r and θ directions because of the width gap which increases as the radius increases too. As this paper aims to deal with unsteady flow, we modify the primary flow so that the angular velocity depends on the radius in the following way:

$$U_\varphi = r \sin\theta \omega(r, \theta, t). \tag{2.2}$$

Such a velocity field is more realistic but as the first one (Eq. (2.1)), it cannot be used to describe the secondary flow and the edge effects. Referring to the literature presented in the introduction, as it is assumed that in this paper all the fluids are purely viscous and that the cone angle remains small, neglecting these disturbing phenomena could be a good approximation. However the following question arises: during the start-up motion is this reasoning still valuable?

Adams and Lodge [8] give an approximate calculation of the pressure gradient due to the centrifugal forces during steady state. That pressure gradient which is proportional to the radius gives rise to the secondary flow. An order of magnitude of that secondary flow with regard to the primary flow is obtained by comparing the two tangential stresses $\tau_{\theta\varphi}$ and $\tau_{r\theta}$ and one can recognize the non-dimensional number Re^*, which has been introduced in perturbation methods to characterize the secondary motion in Turian's paper [18] and is the ratio of these two stresses:

$$R_e^* = \frac{\tau_{r\theta}}{\tau_{\theta\varphi}} = \frac{\rho R\omega^2 R\psi_0}{\frac{\mu\omega}{\psi_0}} = \frac{\rho\omega R^2\psi_0^2}{\mu}\cdot \tag{2.3}$$

During the start up motion, only a part of the fluid near the rotor is moving. This part represents a small ratio $\alpha r\psi_0$ of the total gap. So, as previously we can introduce a new non-dimensional number R^*_{trans}:

$$R^*_{trans} = \alpha^2 R_e^* < R_e^* \tag{2.4}$$

which characterizes the secondary flow during the diffusion process. Therefore, if the secondary flow can be neglected in steady state, this argument is necessarily available during the start up motion.

For the free surface deformation, the answer is not obvious. Indeed, we can imagine complex deformations during this period, perhaps with pulsation of the boundary. The theoretical treatment of these edge effects appears to be very complicated and as such we decided to neglect these effects during the transient period.

3 Governing equations and boundary conditions

In not dealing with normal stress effects, the behaviour of the fluid can be describe by a relationship between $\prod$ and $\mathcal{D}$, the stress and rate of straining tensors, respectively. After having laid down the principle of material objectivity, a non-linear relation $\prod = f(\mathcal{D})$ can be proposed, where f is an isotropic symmetric tensor function. For more details, see the book of Astarita and Marucci [29]. In fact,

this equation assumes that the state of stress at any point at a given time is entirely determined by the strain rate at that point, at the same time. A theorem of tensor analysis states that any isotropic symmetric tensor function $f(\mathcal{D})$ can only be of the form:

$$f(\mathcal{D}) = K_0\mathbf{I} + K_1\mathcal{D} + K_2\mathcal{D}^2 \tag{3.1}$$

where the K_i's are scalar functions of $\mathcal{D}_I$, $\mathcal{D}_{II}$, $\mathcal{D}_{III}$ the three principal invariant values of $\mathcal{D}$.

This is the Reiner-Rivlin model [29]. The K_i's denote the material functions of the fluid. Actually, the Reiner-Rivlin model is not easy to apply because one must experimentally determine the K_i's material functions. Furthermore, that model fails in predicting the normal stress differences of a purely viscous fluid.

Usually, for purely viscous fluids, the generalized Newtonian model is preferred. In this paper, only the specific material function named the apparent viscosity, is considered to be relevant.

Consequently, in the following we shall use the constitutive definition of the generalized Newtonian fluid:

$$\Im = 2\mu(\mathcal{D}_{II})\mathcal{D}, \tag{3.2}$$

where $\Im$ denotes the deviatoric stress tensor and μ the fluid's apparent viscosity. Rigorously, the viscosity material function can only be determine thanks to a viscometric flow. In particular, the unsteady flow in a cone and plate geometry cannot be considered rigorously as a viscometric flow. Nevertheless, considering our velocity field (Eq. (2.2)), the resulting strain rate tensor $\mathcal{D}$ has only two non-zero components: $\dot{\varepsilon}_{\theta\varphi}$ and $\dot{\varepsilon}_{r\varphi}$. So, the first invariant tensor ($\mathcal{D}_I$) and the third one ($\mathcal{D}_{III}$) are identically zero respectively because of the incompressibility condition and the velocity field of the flow. In that case, the concept of generalized Newton fluid seems to be a valuable approximation.

In dealing with time dependent constitutive laws, the time restriction will be removed but the space limitation will be kept.

Necessary equations are:

- the equation of continuity expressed in spherical co-ordinates

$$\frac{\partial\rho}{\partial t} + \frac{\partial(\rho U_r)}{\partial r} + 2\frac{\rho U_r}{r} + \frac{1}{r}\frac{\partial(\rho U_\theta)}{\partial\theta} + \rho U_\theta\frac{\cot\theta}{r} + \frac{1}{r\sin\theta}\frac{\partial(\rho U_\varphi)}{\partial\varphi} = 0 \tag{3.3}$$

  for the considered velocity field, this equation is identically satisfied;
- the dynamic equation.

  In the case where the single volume force due to gravity is neglected, the momentum equation is reduced to:

$$\mathbf{div}(-p\mathbf{I} + \Im) = \rho\left(\frac{\partial\mathbf{U}}{\partial t} + \mathbf{U}\,\mathbf{grad}\,(\mathbf{U})\right). \tag{3.4}$$

In spherical co-ordinates, the following system of equations is obtained:

$$-\frac{\partial p}{\partial r} = \rho\frac{(U_\varphi)^2}{r} \tag{3.5}$$

$$-\frac{\partial p}{\partial\theta} = \rho(U_\varphi)^2\cot\theta \tag{3.6}$$

$$\frac{1}{r^3}\frac{\partial}{\partial r}(r^3\tau_{r\varphi}) + \frac{1}{r\sin^2\theta}\frac{\partial}{\partial\theta}(\tau_{\theta\varphi}\sin^2\theta) = \rho\frac{\partial U_\varphi}{\partial t}\cdot \tag{3.7}$$

It is easily seen that the velocity field U_φ does not satisfy the pressure equations (3.5) and (3.6). Later in the development of the model, only equation (3.7) is considered. This represents our approximate modeling of the flow;

- Boundary conditions.

  In order to solve equation (3.7), one must specify boundary conditions and initial conditions. In this work, we are interested in fluid flow between a rotor (cone) moving at imposed rotation speed and a stator (plate). So we can write:

$$\omega(r,\,\frac{\pi}{2} - \theta_0) = \omega_0(t) \tag{3.8}$$

$$\omega(r,\,\frac{\pi}{2}) = 0. \tag{3.9}$$

We may mention at this point that the use of spherical co-ordinates allows us to distinguish two points physically identical for which the rotation speeds are different. These points are at the extremity of the cone and at the point at the same position on the plate which have different angles in the spherical co-ordinates system.

Concerning free liquid boundary surface, the tangential stress is assumed to be zero:

$$(\Im\cdot\mathbf{n}_r)\cdot\mathbf{n}_\varphi = (\Im\cdot\mathbf{n}_r)\cdot\mathbf{n}_\theta = 0 \tag{3.10}$$

for $r = R$ and $(\frac{\pi}{2} - \theta_0) \leq \theta \leq \frac{\pi}{2}$.

$\mathbf{n}_r$ is the outwards unit normal vector to the free surface. The condition of zero tangential traction leads to $\dot{\varepsilon}_{r\varphi}$ equal to zero at the boundary. There is no assumption about normal traction at the boundary, because the pressure equations are not verified in the domain.

The control volume formulation developed by Patankar [27] was chosen to solve numerically the problem. The details of the numerical strategy is proposed in the first paragraph (Sect. A.1) of the appendix.

4 Results and interpretations

Here we present some numerical results obtained with a regular mesh (usually a 30 by 30 grid). As previously mentioned, the tests were carried out at constant imposed rotation speed. The flow establishment period is analyzed for different fluids: Newtonian, power law and thixotropic.

In order to compare all the results, the different fluids characteristics are chosen to obtain roughly the same

equilibrium apparent viscosity. In that paper, dimensionless presentation is used only to clarify the results and not to solve the problem. All the dimensionless quantities are obtained by dividing the time dependent quantity by the corresponding equilibrium value.

In the first test, the rotor is instantaneously rotated with a constant angular velocity. This condition is not realistic in practice, because it induces an infinite shear rate at initial time. Nevertheless, when the diffusion time of a fluid is much greater than the establishment time of rotor rotation, this leads to a good approximation of the flow.

In the following tests, the rotor is set into motion gradually with the angular velocity given by:

$$\omega = \omega_0 \frac{t}{T}(2 - \frac{t}{T}) \qquad 0 \le t \le T$$
$$\omega = \omega_0(t) \qquad t \ge T. \tag{4.1}$$

Concerning the Newtonian fluid, in the appendix (Sect. A.2) a comparison of the numerical results with two classical analytical solutions is proposed.

4.1 Newtonian fluid [tests 1 and 2]

A first step in the study is the analysis of Newtonian fluid. Figure 2 shows the dimensionless velocity field in the gap at various dimensionless times for an instantaneous rotation. The dimensionless velocity is obtained by dividing the velocity field by the equilibrium velocity of the rotor. The dimensionless time is obtained by dividing the time t by the mean diffusion time

$$\tau = \frac{\rho(\psi_0 R)^2}{2\mu} \cdot \tag{4.2}$$

On the first map, at the beginning of the diffusion process, the velocity gradient is very large near the cone (rotor) and close to zero anywhere else. Then the movement continuously diffused through the gap. Steady state is attained only after a certain time. It can also be observed that the time, required for the flow establishment, depends on the radius. Indeed, near the rotation axis, flow diffusion is quite rapid and the velocity profile quickly becomes a linear function of θ. On the second map, the movement is established for any dimensionless radius R^* less than 0.3, while the fluid is motionless for points with a radius R^* greater than 0.8. At steady state, the curvature of the velocity profile vanishes.

The time evolution of the dimensionless strain rate component in the $\theta\varphi$ directions, clearly shows the different diffusion times as a function of radius (Fig. 3a). The dimensionless strain rate is the ratio of $2\dot{\varepsilon}_{\theta\varphi}(r,\, \theta,\, t)$ and the mean shear rate ω_0/ψ_0. For a given radius, it is assumed that the transient period ends when the discrepancy between cone and plate shear rates becomes negligible (for instance, less than 0.01). The time observed for each radius is in good agreement with the general expression for the diffusion time ($\tau = \frac{\rho(\psi_0 r)^2}{2\mu}$).

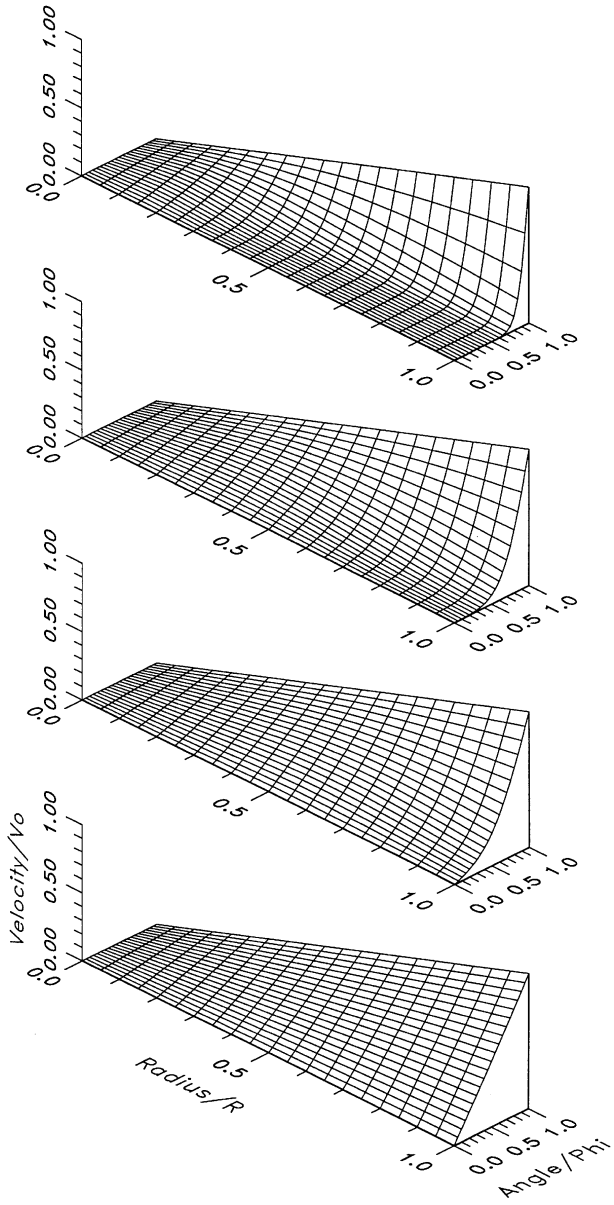

Fig. 2. Test No 1: Newtonian fluid and an instantaneous start-up motion. Dimensionless velocity field at different moments.

Usually, for the imposed rotation speed device, the torque is the single source of experimental information. In the case of the cone and plate geometry, this torque is a source of global information which ignores local effects. In fact, the following expression reveals that the torque evolution is a weighted average of diffusion process at each radius (Fig. 3b):

$$M_v(\theta,\, t) = \int_0^L 2\mu(r,\, \theta,\, t)\dot{\varepsilon}_{\theta\varphi}(r,\, \theta,\, t) 2\pi r^2 \sin^2\theta \, dr. \tag{4.3}$$

The second test is identical to the first one, except for the rotor start up motion which is achieved progressively (Fig. 4). Here, physically admissible results are obtained because deformation rates and torque remain limited (Fig. 5). The deformation rate curves near the cone

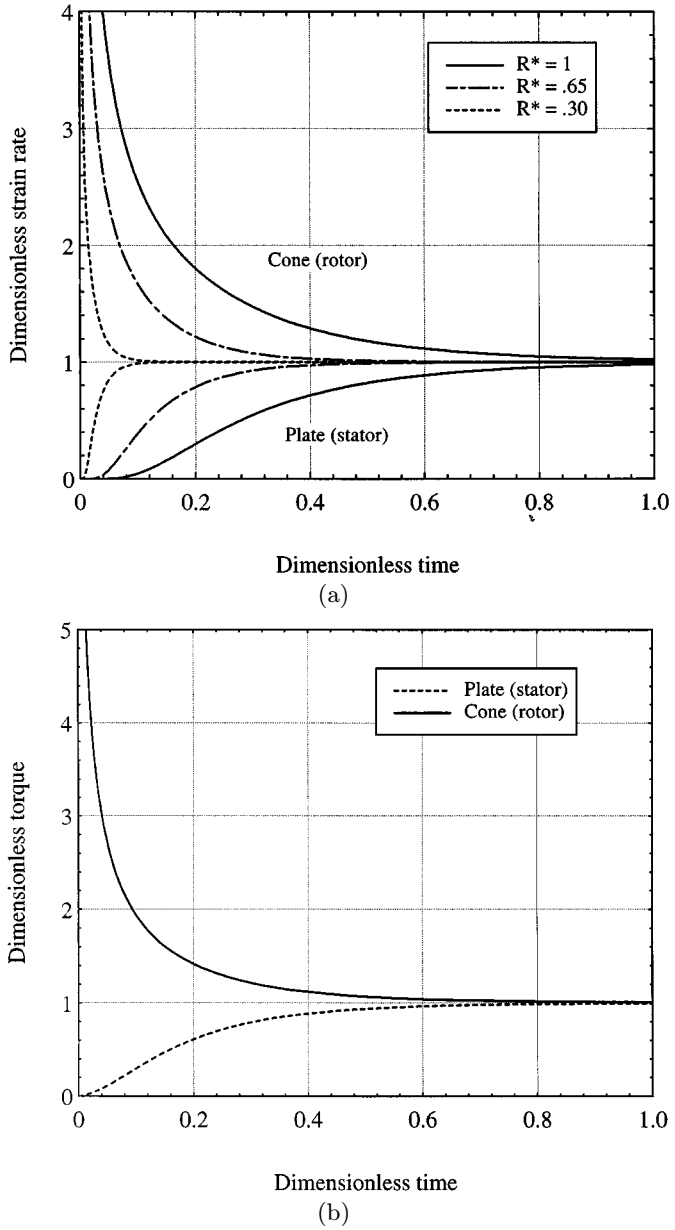

Fig. 3. Test No 1: Newtonian fluid and an instantaneous start-up motion. The dimensionless strain rates and the dimensionless torque calculated on cone and plate.

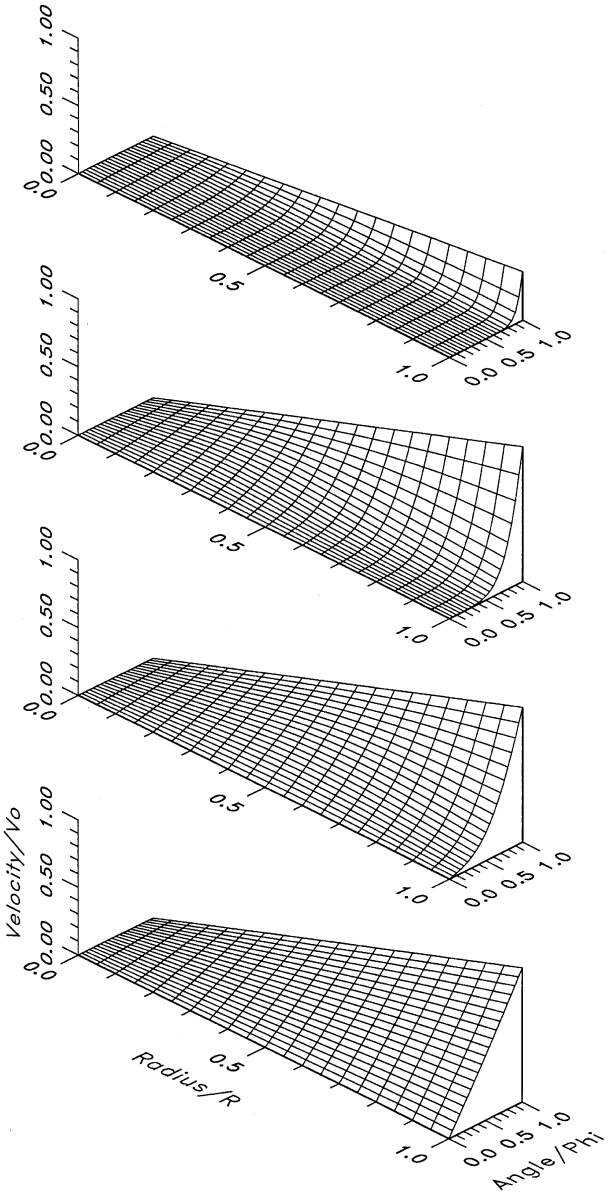

Fig. 4. Test No 2: Newtonian fluid and progressive start-up motion. Dimensionless velocity field at different times.

(rotor) show an "overshoot". This result is in agreement with the one obtained for a coaxial cylinder and parallel plate geometry, see the papers of Kouitat *et al.* [1,2] and Okeson and Emery [4]. This overshoot is due to the excess of torque necessary to overcome fluid inertia (Fig. 5b). The overshoot magnitude is strongly related to the ratio of flow diffusion time to the establishing time of rotor motion and increases with radius (Fig. 5a).

Concerning the torque curves, one notices that only the rotor torque reveals an overshoot. Let us recall that the torque is an average of local tangential stress, weighted by the squared radius (Eq. (4.3)). The area between the curves of cone and plate torque is proportional to the difference of rotating momentum between transient and steady states. Consequently, for the same density and same geometrical parameters (angle, radius, velocity), the whole area separating the torque curves does not depend on the viscosity nor the behaviour law. Actually, we will see that the viscosity function changes only the shape of this area: higher overshoot (for the torque, not necessary for the strain-rate) and shorter transient period as the viscosity increases.

The calculation using the approximated diffusion coefficient ($\tau = \frac{\rho(\psi_0 R)^2}{2\mu}$) in the following case ($\mu = 50 \times 10^{-3}$ Pa s, $\rho = 800$ kg m^{-3}, $\psi_0 = 3°$, $2R = 7.5$ cm) gives a value of about 31 ms and the code gives a value of 21 ms. This last value is calculated thanks to the test: $|\text{torque}_{\text{plate}} - \text{torque}_{\text{cone}}| \leq 0.01$.

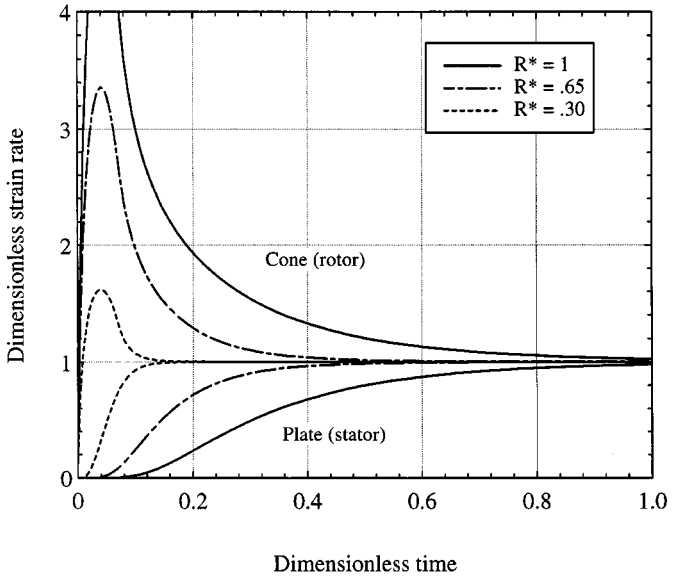

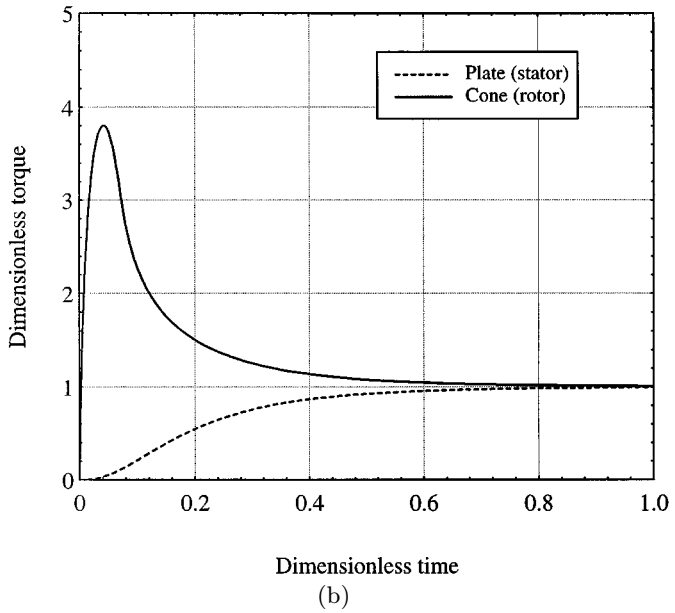

Fig. 5. Test No 2: Newtonian fluid and progressive start-up motion. The dimensionless strain rates and the dimensionless torque calculated on cone and plate.

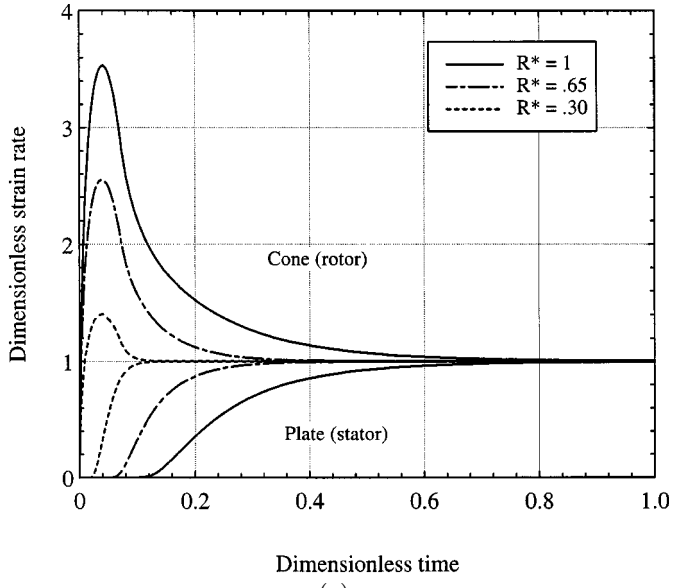

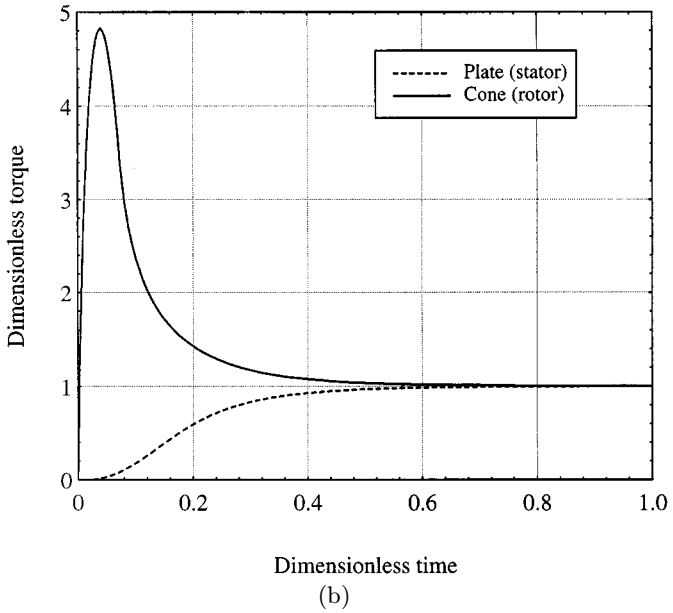

Fig. 6. Test No 3: Shear-thickening fluid ($n = 1.5$). The dimensionless strain rates and the dimensionless torque calculated on cone and plate.

4.2 Power law fluids [tests 3 and 4]

The power-law model is generally expressed in the following way:

$$\Im = K(\mathcal{D}_{II})^{\frac{n-1}{2}}\mathcal{D} \tag{4.4}$$

where n and K are constant parameters called the power law index and the consistency respectively.

When the value of n is less than 1, the material is shear thinning as the apparent viscosity decreases when the shear rate increases. In the other case the material is shear thickening.

In our calculations we have used values of n equal to 1.5 and 0.3. For each of these values, the consistency K is chosen so that at steady state the apparent viscosity is the same as the one used for Newtonian fluids (tests 1 and 2).

The power law fluids (Fig. 6 and Fig. 7) shows during start up motion similar phenomena to that exhibited by Newtonian fluids. For example, diffusion times are less important near the rotation axis. Due to the dependency of the apparent viscosity on the strain rate, some specific phenomena appear.

– The shear-thickening fluid (Fig. 6):
The rotor start up motion generates fluid layers in its vicinity, where the strain rate and the apparent viscos-

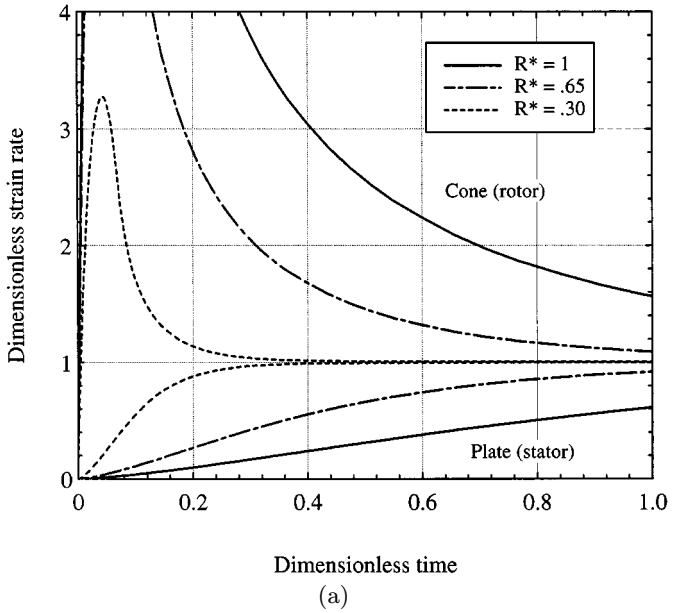

(a)

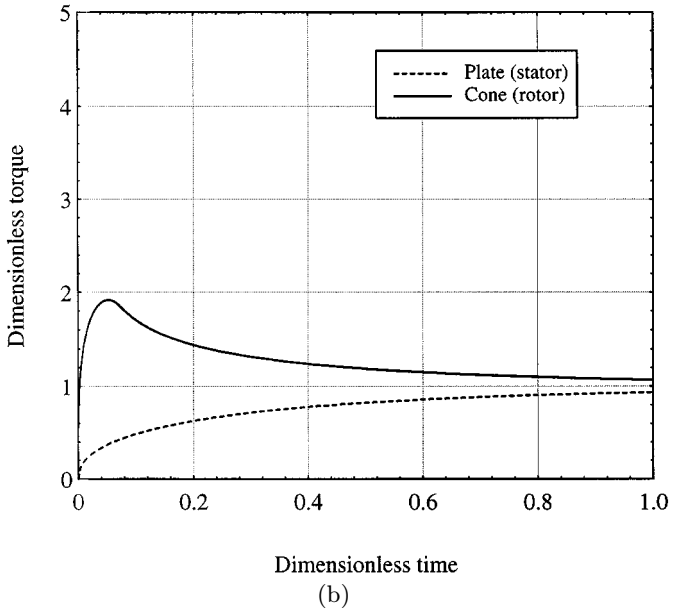

(b)

Fig. 7. Test No 4: Shear-thinning fluid ($n = 0.3$). The dimensionless strain rates and the dimensionless torque calculated on cone and plate.

ity values are very high. As a result, the movement diffuses very quickly within the fluid. So, the moving fluid layers transmit a large shear stress to unmoving fluid, for which apparent viscosity is very low. This way of start up motion proves very efficient. Compared with the Newtonian case (test 2), the strain rate overshoot is lower, while the high apparent viscosity induces a more emphasized torque overshoot. It is also observed that at short times, the cone torque is very large because the high shear rate near the cone, generates high fluid viscosity. Consequently, the power necessary to move the cone (rotor) is very large at the beginning of the transient period. Regarding the stator torque on the plate, one notices that its value and that of its derivative are zero for short times. This is due to the low viscosity of the unmoved part of the fluid which generates a poor diffusion process towards the stator.

– The shear-thinning fluid (Fig. 7):
Here, the process is the opposite: the moving and unmoving fluid layers possess a low and high viscosity, respectively. So, the start up motion is very slow. The strain rates are very high and decrease slowly with time. In order to compensate this phenomenon, the resulting torque is greatly reduced and the overshoot is not very marked.
At $t^* = 0$, the derivative of the stator torque is almost infinite. This phenomenon is a consequence of the high viscosity of the unmoved part of fluid, which very quickly transmits the movement from the rotor to the stator.

4.3 Time-dependent fluid [test 5]

In this section, the flow of a time-dependent fluid is analyzed. The Cross model combined with a kinetic equation proposed by Cheng [30], allows us to characterize "thixotropic" fluids. Consequently, the stress at any time is not completely determined by the strain rate at that time. In order to remove the time restriction, the constitutive equation is modified to include a structure parameter λ accounting for time-dependent effects. λ is an additional internal variable which characterizes the material structure and ranges from zero to one.

Assuming that the decay of the structural parameter with time follows a kinetic equation as:

$$\frac{d\lambda}{dt} = a(1-\lambda) - b(\mathcal{D}_{II})^{\frac{1}{2}}\lambda$$
$$\mu = \mu_\infty + c\lambda \tag{4.5}$$

where the breakdown rate $b(\mathcal{D}_{II})^{\frac{1}{2}}\lambda$ depends on strain rate and the build-up rate a $(1-\lambda)$ depends on the amount of structure to be recovered.

For test 5, the parameters are chosen in order to obtain the Newtonian viscosity value at the equilibrium:

$$a^* = 5 \times 10^{-5} \qquad b = 4 \times 10^{-3}$$
$$\mu_\infty = \mu_{eq} \qquad c = 2\mu_{eq}$$

with the initial condition: $\lambda(t^* = 0) = 1$ and where $a^* = \frac{a\psi}{\omega_0}$.

Figure 8a presents the evolution of strain rates. It can be observed that at the beginning of the diffusion process, the thixotropic fluid behaves like the Newtonian fluid of test 2 with a much higher viscosity. Afterwards, the strain rate curves stay distant from each other and converge very slowly to the equilibrium state. The heterogeneity of the structure breakdown throughout the fluid sample is responsible for this phenomena. Indeed, for a given radius the history of the fluid is different near the rotor compared near the stator. Consequently, the equilibrium values of the deformation rate respectively on the rotor and

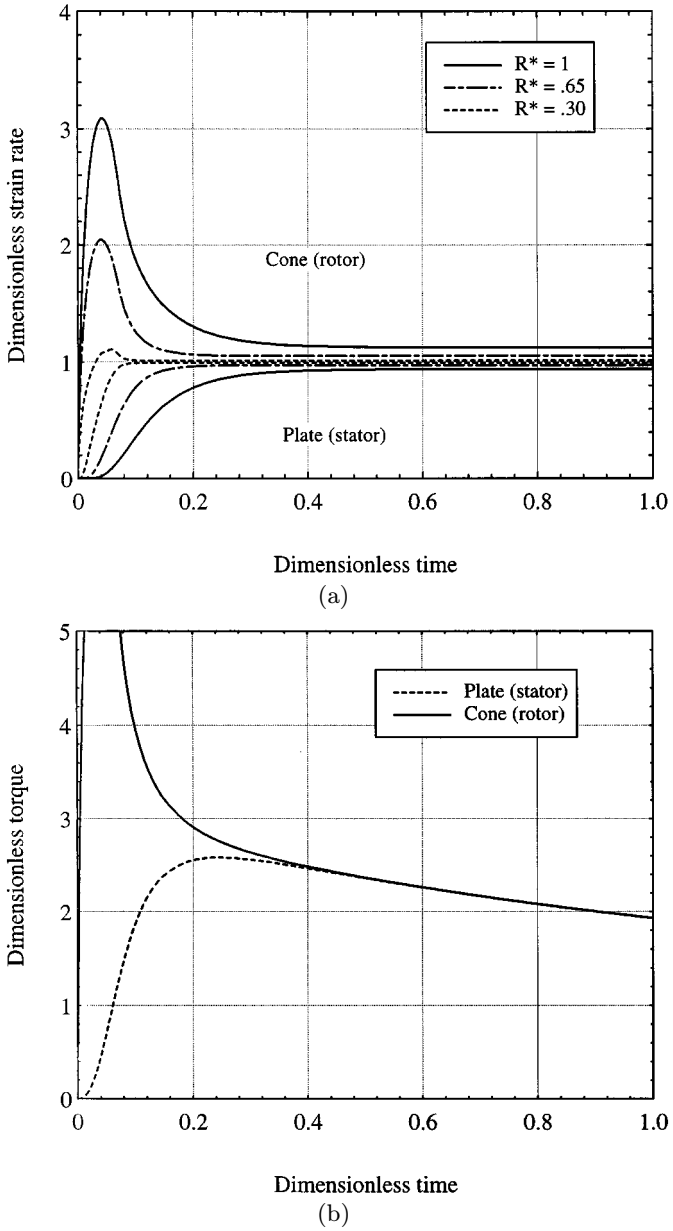

Fig. 8. Test No 5: Time dependent fluid ($a^* = 5 \times 10^{-5}$, $b = 4 \times 10^{-3}$) The dimensionless strain rates and the dimensionless torque calculated on cone and plate.

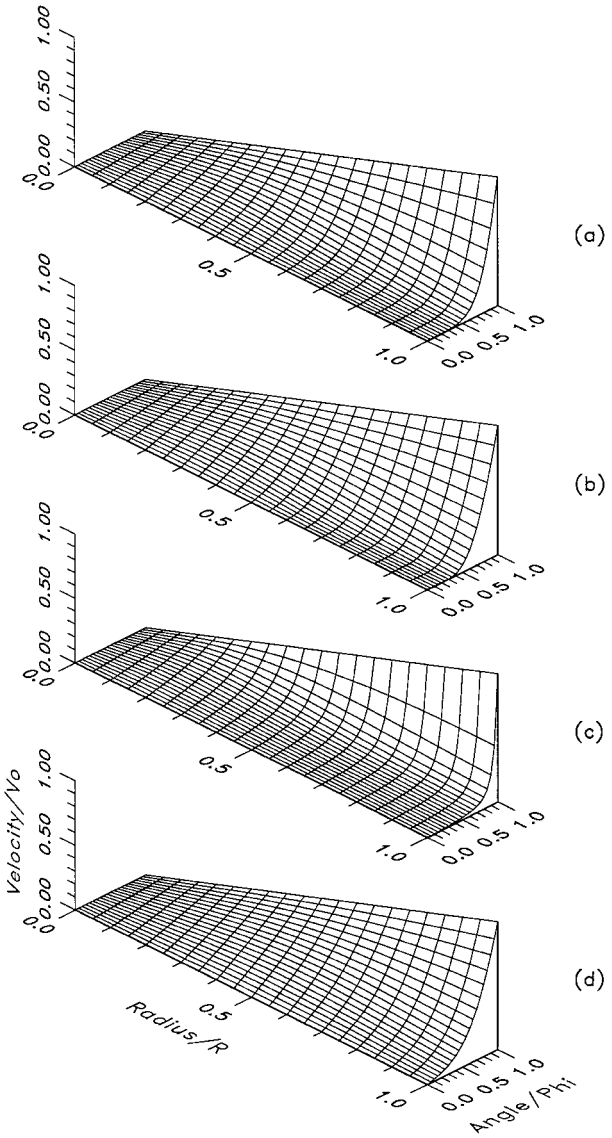

Fig. 9. The fluid rheology influence: Dimensionless velocity field at $t^* = 0.07$ for the tests No 2, 3, 4 and 5.

on the stator remain different. This analysis is confirmed by the evolution of the torque values (Fig. 8b). Indeed, after the dimensionless time 0.4, the torque curves approach each other and when they join up, the fluid inertia becomes negligible. Then, during a quasi-stationary period, the breakdown of the structure leads to a decrease of the two torque values. The overshoot observed on the stator torque curve is very relevant: one can state that it characterizes a thixotropic fluid.

Figure 9 gives the velocity profiles at the same time ($t^* = 0.07$) for the Newtonian, shear-thickening, shear-thinning and thixotropic fluids. On that figure, one can observe that the diffusion process strongly depends on the fluid characteristics. For the thixotropic fluid despite of being very close of the end of the diffusion process, the velocity profiles remain non linear in function of the cone angle ψ. This phenomena is due to the strain rate field which remains non uniform throughout the gap as the inertia effect vanishes.

4.4 Discussion

At this stage, we built a numerical code as a rheometrical tool which can help us to better understand the flow of complex fluid in a cone and plate geometry. The approached model does not allow us to deal with the secondary flow or with the free surface deformation. In return, it enables the study of the transient period during start up motion and emphasizes the specifications of the diffusion process in the cone and plate geometry.

An important step in establishing a feasible and suitable simulation code has been the adaptation of the control volume method to a spherical co-ordinate problem with tensorial values.

In the case of a speed driven instrument, the numerical results obtained for different constitutive laws, exhibited some very relevant phenomena:

- One of the specifications of the cone and plate geometry is that the time diffusion of fluid motion varies with respect to the radius. Hence, the experimental measurement (*i.e.* the torque) is only an average information of the flow complexity.
- It is very important to emphasize the difference between Newtonian and non Newtonian fluids. In the second case, it is absolutely forbidden to use the equilibrium viscosity in order to determine the unsteady period. Indeed, it would be a big mistake. In Figure 9, considering the four velocity profiles points out four different ways of reaching the steady state for a same equilibrium viscosity.
- A torque overshoot, which is specific to time-dependent fluids, can be observed on the stator.

In the following part of this paper, a comparison of the code results and experiment will demonstrate how the code has to evolve to take into account the specificity of the apparatus and can improve the analysis of the rheometrical results.

5 Experiment

This paragraph introduces the second part of the paper, for which a comparison between numerical results and experiment is proposed. The experimental tests are carried out on a Weissenberg rheometer which is presented in the appendix (Sect. A.3).

Firstly, the code is tested for three Newtonian fluids:

$$\mu_1 = 117 \text{ mPa s}$$
$$\mu_2 = 1929 \text{ mPa s}$$
$$\mu_3 = 13878 \text{ mPa s}.$$

The tests are carried out under the following conditions:

$$\omega_1 = 3.49 \text{ rd s}^{-1}$$
$$\omega_2 = 1.05 \text{ rd s}^{-1}$$
$$\omega_3 = 0.07 \text{ rd s}^{-1}.$$

Figure 10a shows the time evolution of the measured torque for the fluid with viscosity μ_1. The numerical results obtained for the same conditions are presented in Figure 10b. In this Figure, the lower curve represents the evolution of the stator torque calculated with the code "RHEOUTIL". The single common value to the experimental and numerical curves is the equilibrium value of the torque. The curve shapes and the time order of magnitude are completely different. Indeed, the ratio of the two

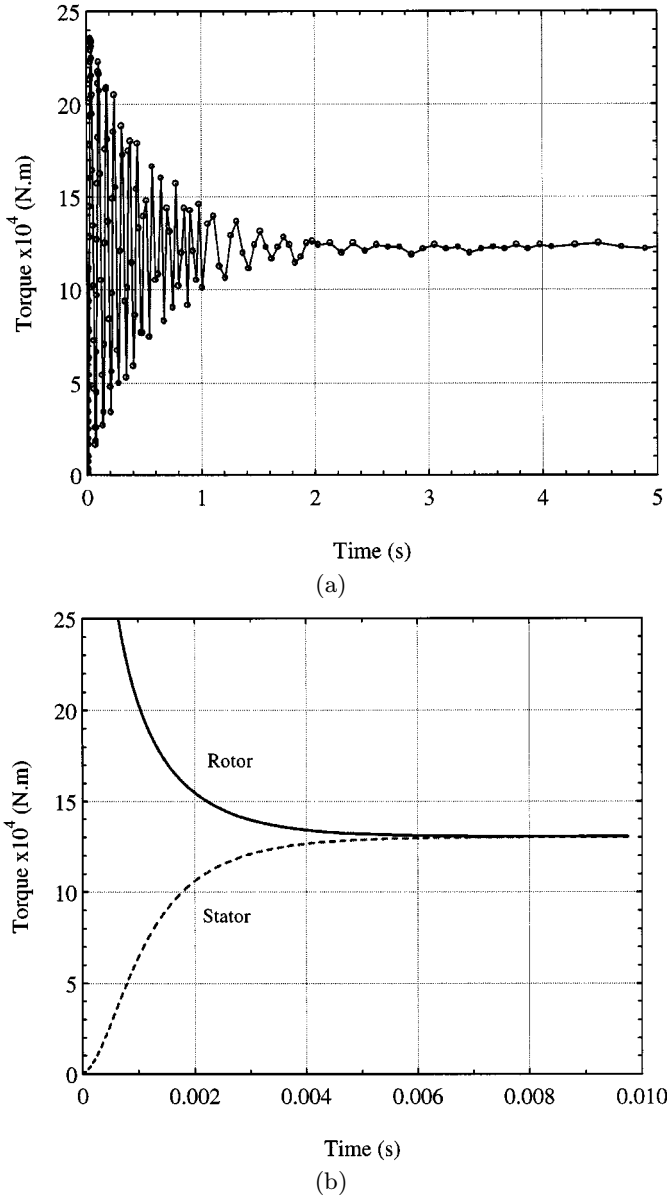

Fig. 10. The time evolution of the torque for a Newtonian fluid ($\mu = 117 \times 10^{-3}$ Pa s, $\rho = 874$ kg m^{-3}). (a) experimental result; (b) code result.

time constants is of the order of 10^3 and one can observe oscillations on the experimental curve. This can be easily explained if we remember that not the fluid torque but the torsion angle of the bar is measured (see Sect. A.3). The response of this torsion bar with time results from a fluid structure interaction.

Observing the results obtained for the second fluid (Fig. 11a), one can note that the frequency of the oscillations remains very close to the frequency of the free oscillations of the system (stator and torsion bar) which can be deduced from the following equation:

$$-k\alpha = I\frac{d^2\alpha}{dt^2} \tag{5.1}$$

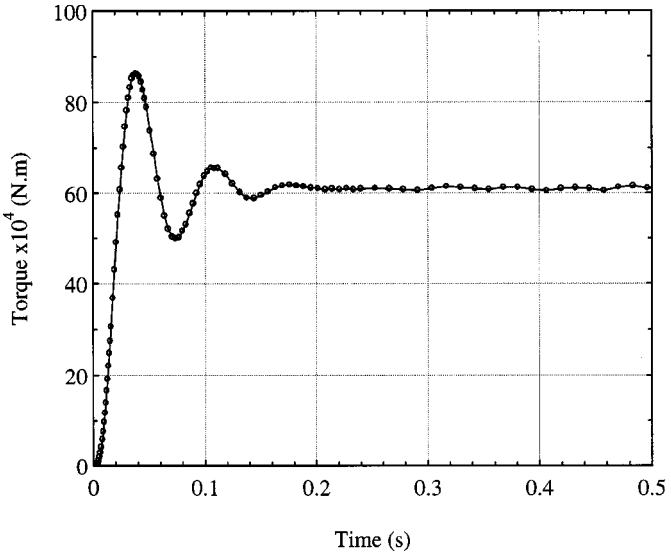

(a)

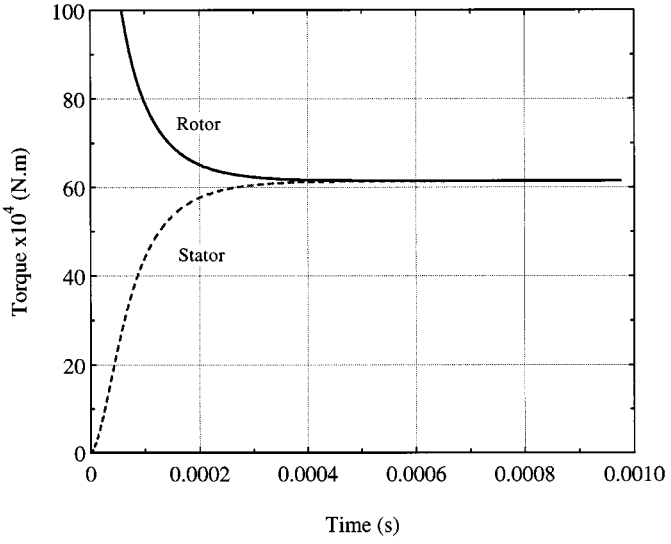

(b)

Fig. 11. The time evolution of the torque for a Newtonian fluid ($\mu = 1929 \times 10^{-3}$ Pa s, $\rho = 908$ kg m^{-3}). (a) experimental result; (b) code result.

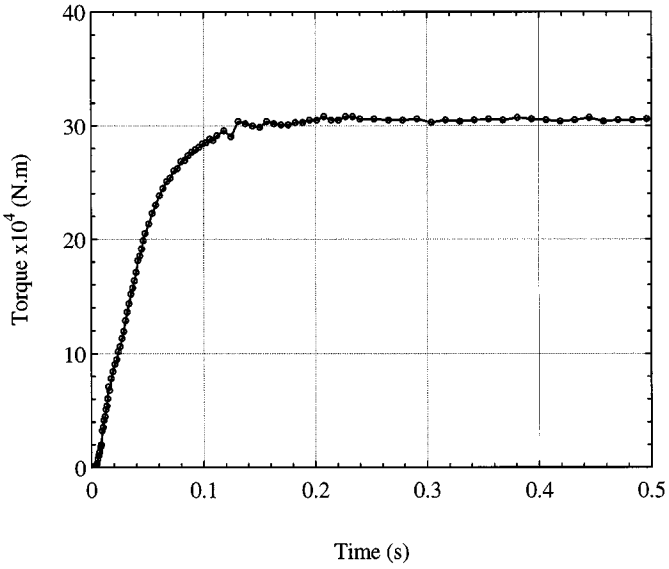

(a)

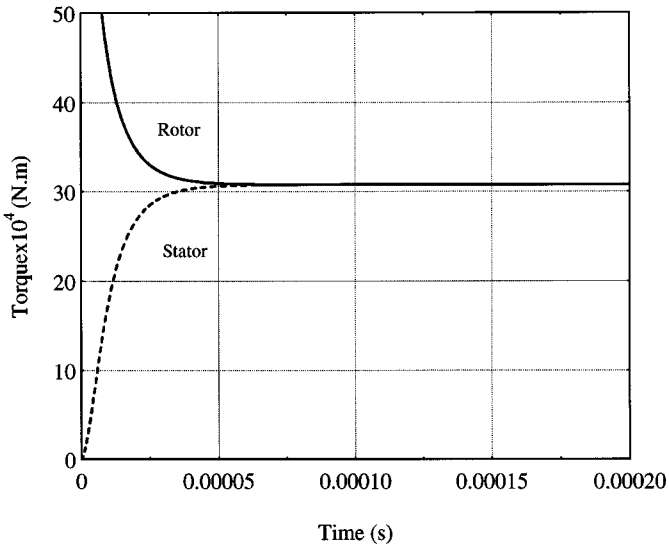

(b)

Fig. 12. The time evolution of the torque for a Newtonian fluid ($\mu = 13878 \times 10^{-3}$ Pa s, $\rho = 887$ kg m^{-3}). (a) experimental result; (b) code result.

and is given by the following expression:

$$N_0 = \frac{1}{2\pi}\sqrt{\frac{k}{I}}\,. \tag{5.2}$$

The analytical expression presented in paragraph 7, will confirm that the frequency shift due to the fluid viscosity is in fact very small. At the opposite, the way the oscillations are damped out depends strongly on the fluid rheology. In particular, the oscillations can even disappear for a very viscous fluid (Fig. 12a).

Note that, on the experimental results presented in Figure 10a, the frequency seems to decrease after about one second. This is only a artefact due to the apparatus: in order to reduce the data file size, the sampling frequency is automatically reduced after a certain time. In that case of low viscous fluid, the Shannon's theorem is not respected. Indeed, the sampling frequency must exceed twice the signal bandwidth in order for the original signal to be recoverable from the sampled signal [31]. This problem disappears for the other fluids because the time constant of the process decreases as the viscosity increases.

Figures 10b, 11b and 12b depict the results calculated with the model presented previously, for viscosity values μ_1, μ_2 and μ_3 respectively. Observing the stator torque, it is obvious that neither the curve shape nor the time scale are in agreement with the measurements. Consequently, it is necessary for the model to account for the mechanism due to the fluid structure interaction. This is the aim of the next paragraph.

6 Formulation of the fluid structure interaction

6.1 Moving stator

Due to the fluid structure interaction, the stator cannot be assumed motionless. If α stands for the bar angle, the new boundary conditions become:
on stator

$$\omega(r, \frac{\pi}{2} - \theta_0) = \frac{d\alpha}{dt} \tag{6.1}$$

and on rotor

$$\omega(r, \frac{\pi}{2}) = \omega_0(t) \tag{6.2}$$

where $d\alpha/dt$ is obtained by solving the differential equation describing the bar movement:

$$-k\alpha + M_v = I\frac{d^2\alpha}{dt^2} \tag{6.3}$$

M_v denotes the viscous torque which is the damping term of the equation.

6.2 Numerical strategy

The code described in the first part has been improved in order to deal with the coupling which arises between the velocity field in the fluid and the stator motion. The method of solution for the velocity field is similar to the one described in the first part (Sects. 3 and A.1). As it was previously noted, the time constant of the diffusion process is very different of the time constant of fluid structure interaction. This allows us to treat the coupling using an iterative scheme. The main difference with the previous calculation, is the stator motion given by equation (6.3) and which depends on the viscous torque M_v. Therefore the iterative procedure is realized as follows:

a) The velocity field is calculated thanks to the boundary conditions (Eq. (6.1) and (6.2)) by using the bar movement at the previous time increment as estimated value.
b) This estimated velocity field is used to calculate the viscous torque at the stator (Eq. (4.3)), which allows the bar motion to be solved (Eq. (6.3)).
c) Coming back to a) with the new estimated value of the angular velocity, and on so on until a convergence criterion has been satisfied.

This strategy allows us to preserve a fully implicit scheme without changing the structure of the matrix to be solved at each iteration.

6.3 Results for Newtonian fluids

The results obtained for Newtonian fluid with the viscosity μ_1, μ_2 and μ_3, are presented in Figures 13a, 14a and 15a respectively. A perfect agreement with experimental results can now be observed (refer to Figs. 10a, 11a and 12a) in spite of the very wide range of viscosity values used (117 mPa s up to 13.878 mPa s). This proves the ability of the model "RHEOUTIL" to simulate complex phenomena during unsteady flow.

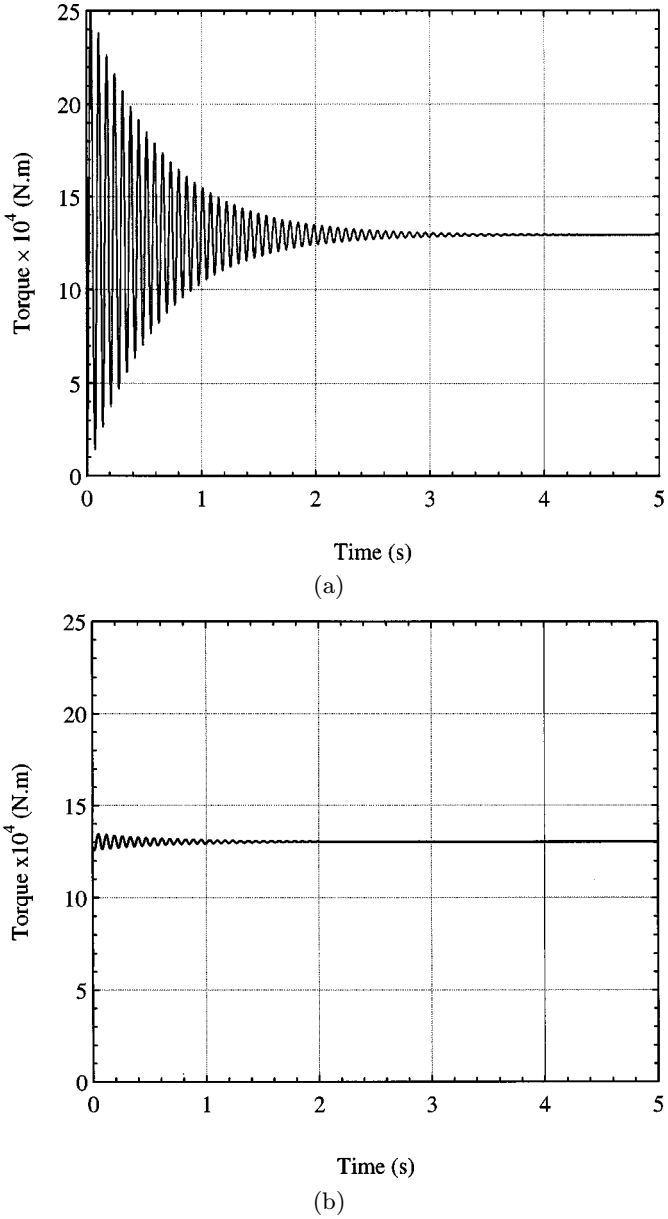

Fig. 13. Simulation of the fluid structure interaction ($\mu = 117 \times 10^{-3}$ Pa s, $\rho = 874$ kg m^{-3}). (a) twist torque $k\alpha$; (b) viscous torque M_v (near the stator).

During the transient period, it is important to mention that the viscous torque M_v is very different from the torsion torque $-k\alpha$: the more important the fluid structure interaction, the more different the two torque curves become. Figures 13b,14b and 15b give the evolution of the viscous torque M_v calculated at the stator. For the lowest viscosity (Fig. 13), the bar angle undergoes oscillations with large magnitude and low attenuation. Nevertheless, the viscous torque is not so perturbed: in this case, the shear strain induced by the bar motion remains weak compared to the one induced by the rotation of the rotor. In spite of the bar oscillations, the fluid structure interaction

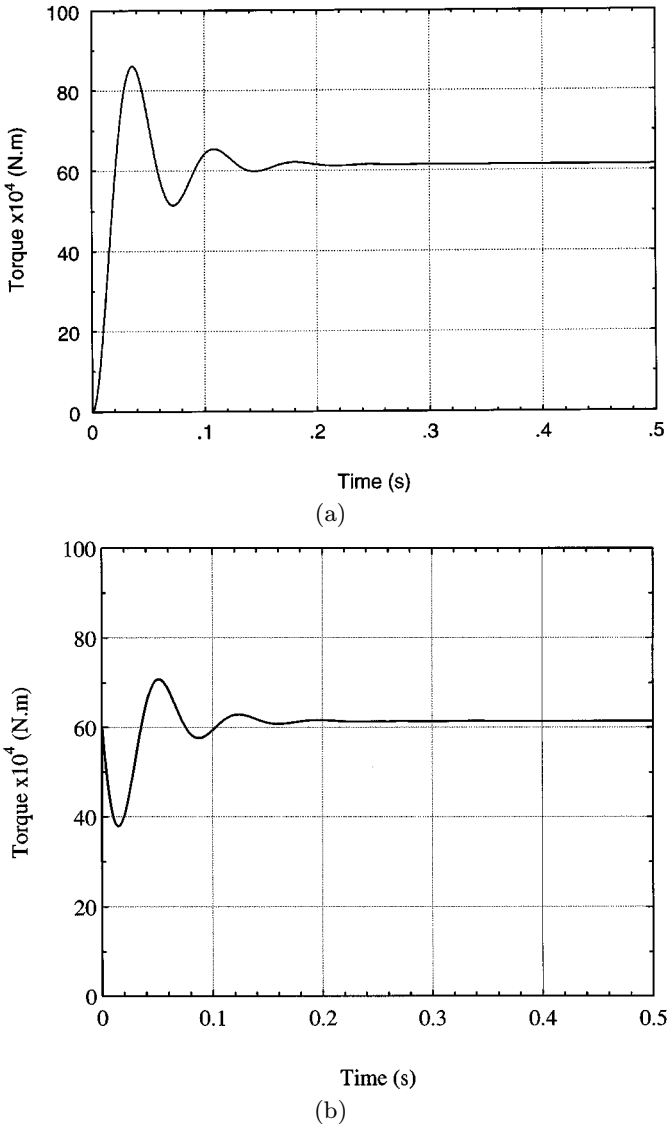

Fig. 14. Simulation of the fluid structure interaction ($\mu = 1929 \times 10^{-3}$ Pa s, $\rho = 908$ kg m^{-3}). (a) twist torque $k\alpha$; (b) viscous torque M_v (near the stator).

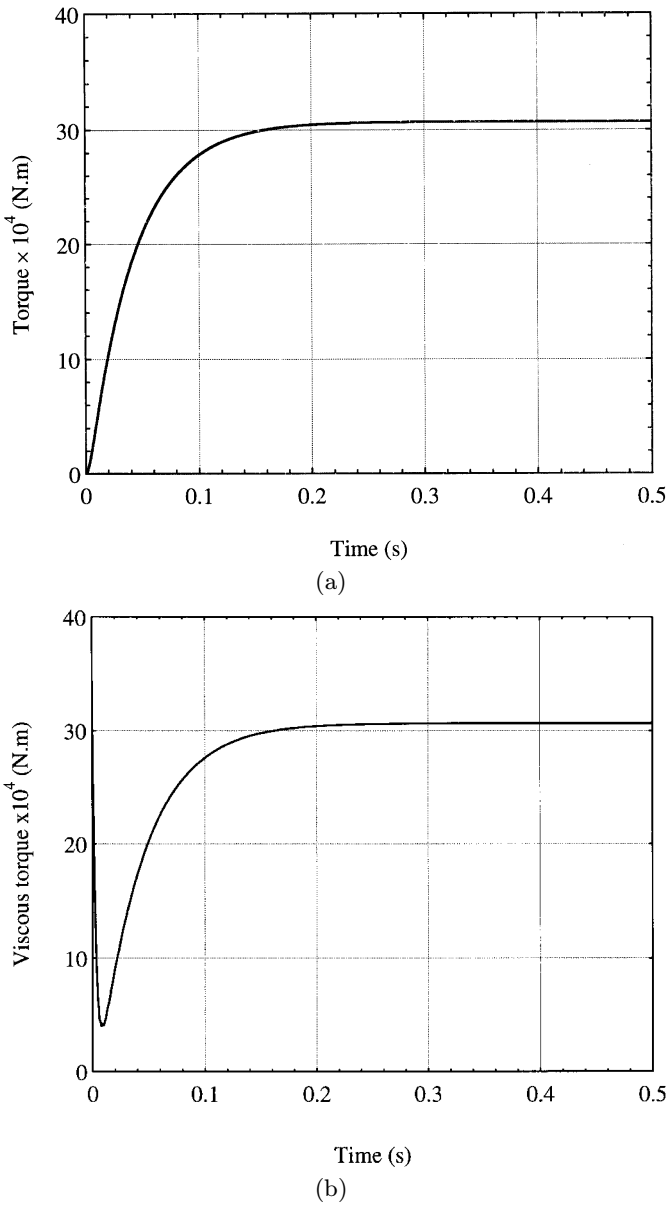

Fig. 15. Simulation of the fluid structure interaction ($\mu = 13878 \times 10^{-3}$ Pa s, $\rho = 887$ kg m^{-3}). (a) twist torque $k\alpha$; (b) viscous torque M_v (near the stator).

is very weak in this case. For viscosity μ_2 (Fig. 14), both the viscous torque and the torque deduced from the bar angle show out important oscillations which reduce much faster. Note that a delay can be observed between these two torque curves. In that case, the motion due to the bar movement begins to be important. For the largest viscosity (μ_3) one can observe the sub-critical regime (Fig. 15). Indeed, the oscillations disappear and the fluid structure interaction modifies dramatically the viscous torque before 0.02 s.

This points out the effects of fluid structure interaction. As main consequence, we must keep in mind that it is not obvious to determine the fluid properties from the measured torque $-k\alpha$, when the unsteady-state has to be used.

Figures 10, 11 and 12 proved that the constant time of the diffusion process in the fluid sample is very small compared with the time scale of the fluid structure interaction. One guesses that taking into account the diffusion process is not necessary in those particular cases. Consequently, an analytical solution using the lubrication assumption is proposed in the following paragraph.

7 Lubrication assumption

7.1 Analytical solution

Results obtained in the previous paragraphs seem to prove that, in usual configurations, the time constant related to the fluid structure interaction is much larger than the time required for the velocity field to be established in the fluid sample. Consequently, the term of inertia is small

in magnitude compared with the viscous torque. In this case, Batchelor [32] propose to use the lubrication theory. By assuming steady-state fluid flow, the physical formulation becomes much simpler: in the equation governing the structure movement (Eq. (6.3)), the fluid torque M_v is calculated using the classical equation that determined the torque obtained in steady-state for a cone and plate geometry. However, the stator is not more at rest here and the shear rate in the fluid sample depends on the bar movement:

$$M_v = \frac{2}{3}\pi L^3 \cos^2(\psi)\frac{\mu}{\psi}\left[\omega - \dot{\alpha}\right]. \tag{7.1}$$

Reporting this expression in the previous equation leads to the well-known formulation of a damping oscillating system:

$$I\frac{d^2\alpha}{dt^2} + J\frac{d\alpha}{dt} + k\alpha = J\omega \tag{7.2}$$

where

$$J = \frac{2}{3}\pi L^3 \cos^2(\psi)\frac{\mu}{\psi}\,.$$

Assuming an instantaneous start up motion of the rotor, the initial conditions simply read:

$$\text{at } t = 0,\ \alpha = 0 \text{ and } \frac{d\alpha}{dt} = 0. \tag{7.3}$$

In the case of Newtonian fluids, a straightforward analytical solution exists. The form of the solution depends on the dumping term magnitude. The latter is characterized by the value of $\Delta = J^2 - 4Ik$.

If $\Delta < 0$, we obtained damped out oscillations:

$$\alpha(t) = \frac{J\omega}{k}\left\{1 - \exp(-at)\left[\cos(bt) - \frac{a}{b}\sin(bt)\right]\right\}. \tag{7.4}$$

If $\Delta > 0$, the system is sub-critic and hence the oscillations disappear:

$$\alpha(t) = \frac{J\omega}{k}\Big\{1 - \frac{a+b}{2b}\exp\big(-(a-b)t\big) + \frac{a-b}{2b}\exp\big(-(a+b)t\big)\Big\} \tag{7.5}$$

in both expressions,

$$a = \frac{J}{2I} \text{ and } b = \frac{\sqrt{|\Delta|}}{2I}.$$

7.2 Results and discussion

The analytical equations (7.4) and (7.5) have been used to calculate the evolution of the bar angle versus time for the three Newtonian fluids defined in paragraph 5. Fluids 1 and 2, with viscosity values of 117 and 1929 mPa s respectively, obey equation (7.4), while the more viscous one (13878 mPa s) generates a sub-critical flow (Eq. (7.5)) as observed on the experimental curve. For all configurations, the analytical solution is in excellent agreement with the experimental and numerical results. This proves that the assumption of steady-flow through the sample remains valid in spite of the large range of viscosity values.

Table 1. Effect of the fluid viscosity on the oscillation frequency.

	Viscosity (mPa s)	**Frequency N (Hz)**	N/N_0
Free oscillations	0	$N_0 = 14.4092$	1
Newtonian fluid 1	117	14.4072	0.99986
Newtonian fluid 2	1929	13.8495	0.961

Thanks to the analytical expressions, some of the previously observed phenomena can be more rigorously analyzed. In particular, as long as the value of discriminant Δ remains negative, the frequency can be deduced from equation (7.4):

$$N = \frac{b}{2\pi} = \frac{1}{2\pi}\sqrt{\frac{k}{I} - \frac{J^2}{4I^2}}\,. \tag{7.6}$$

The second term in the square root stands for the shift in frequency due to the damping coefficient. The values of N obtained for fluids 1 and 2 using this expression are reported in Table 1, as well as the ratio of N over the free oscillation frequency N_0. The very small variation in frequency is consistent to what has been observed on the experimental and numerical results.

In addition, the analytical method allows a criterion to be derived for the validity of the steady state flow assumption. In order to do that, we have to consider the time scales related to the fluid inertia and the fluid structure interaction respectively. The time constant tied to the fluid inertia τ has been discussed in detail in the first part of this paper. It depends on the gap of the fluid sample and on the kinematics viscosity of the fluid:

$$\tau = \frac{\psi^2 R^2 \rho}{2\mu}\,. \tag{7.7}$$

An order of magnitude of the time constant due to the fluid structure interaction T can simply be obtained through the frequency of free oscillations of the system:

$$T = \frac{1}{N} \approx 2\pi\sqrt{\frac{I}{k}}\,. \tag{7.8}$$

A reasonable criterion to be satisfied to ensure that quasi steady flow arises in the fluid sample is to impose the first time constant very small compared to the second one:

$$\frac{\tau}{T} = \frac{\psi^2 R^2 \rho}{4\pi\mu}\sqrt{\frac{k}{I}} \ll 1. \tag{7.9}$$

Table 2. Steady-state criterion calculated for the Newtonian fluids used in this section. The results prove that the assumption of steady-state is almost always valid.

	Density ($\mathrm{kg\,m^{-3}}$)	Viscosity (mPa s)	τ/T
Newtonian fluid 1	874	117	9.5×10^{-2}
Newtonian fluid 2	908	1929	6.0×10^{-3}
Newtonian fluid 3	887	13878	8.2×10^{-4}

As depicted in Table 2, this criterion is almost always satisfied for the Newtonian fluids used in this section. The largest value is obtained for the low viscous fluid, for which the ratio of the two time constant is only one tenth.

This relative high value let us assume that some effects due to unsteady-flow must be observed. Indeed, by analyzing closely the analytical and numerical curves obtained for fluid 1, one can note two differences:

- at very short times (Fig. 16), a delay clearly appears on the curve calculated with the numerical code. The same mechanisms seems to occur with a translation of the time axis. This is simply due to the time required for the motion to diffuse through out the fluid sample (see the first part);
- during the damp out of the oscillations, little differences can also be observed between the two calculations. The numerical results exhibits a slightly faster damped out system and a shift in frequency observable on the derive along the time scale. Both effect looks like a oscillating system with a damp out coefficient just a little larger than the one calculated with the lubrication assumption. This must be analyzed by the velocity gradient at the stator surface. During unsteady-state, the velocity field at the surface is curved instead of linear. This increases the shear rate at the surface, and hence, the viscous torque that acts again the bar movement, responsible for the damping of the oscillations.

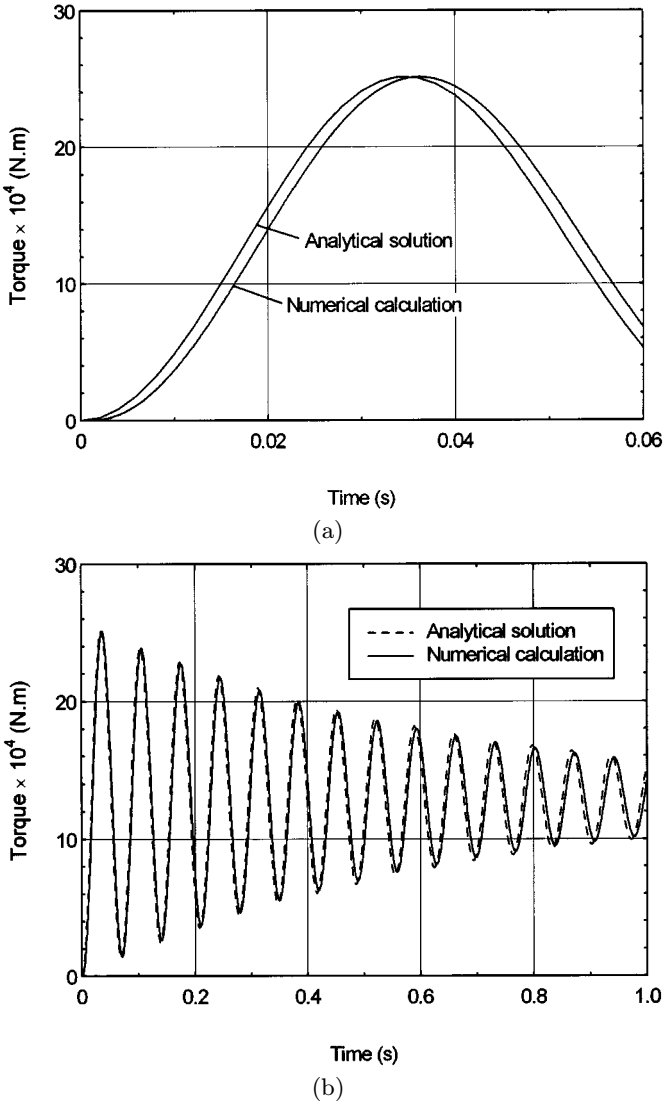

Fig. 16. Comparison of numerical and analytical solution($\mu = 117 \times 10^{-3}$ Pa s, $\rho = 874\ \mathrm{kg\,m^{-3}}$).

8 Analysis for non Newtonian fluids

In this paragraph, the comparison between experiment and simulation gives relevant information about the rheological behaviour of two shear-thinning fluids. It appears very clearly that these non Newtonian fluids exhibit also other rheological properties which can have a non negligible effects during unsteady state process.

8.1 Shear-thinning fluids

In this section, two shear-thinning fluids are tested. The first one which is named fluid A in the following, contains 3% in weight of CMC (Prolabo) dissolved in water and the other one which is named fluid B, contains 2% in weight of CMC (Tylose) dissolved in water. These fluids have been characterized using the following flow procedure: the experiment mode is an equilibrium ramp of about two hours during which the shear rate increases linearly from 1 $\mathrm{s^{-1}}$ up to 70 $\mathrm{s^{-1}}$. For both fluids, the best fit was obtained with the Cross model [33]:

$$\frac{\mu - \mu_\infty}{\mu_r - \mu_\infty} = \frac{1}{(1 + (K\dot{\gamma})^n)} \tag{8.1}$$

μ_r : zero-rate viscosity (Pa s)
μ_∞ : infinite-rate viscosity (Pa s)
K : consistency (s)
n : rate index
$\dot{\gamma}$: shear rate ($\mathrm{s^{-1}}$).

The other advantage of the Cross model over the power law model is to define a finite zero-rate viscosity, which results in a more realistic constitutive model. The following

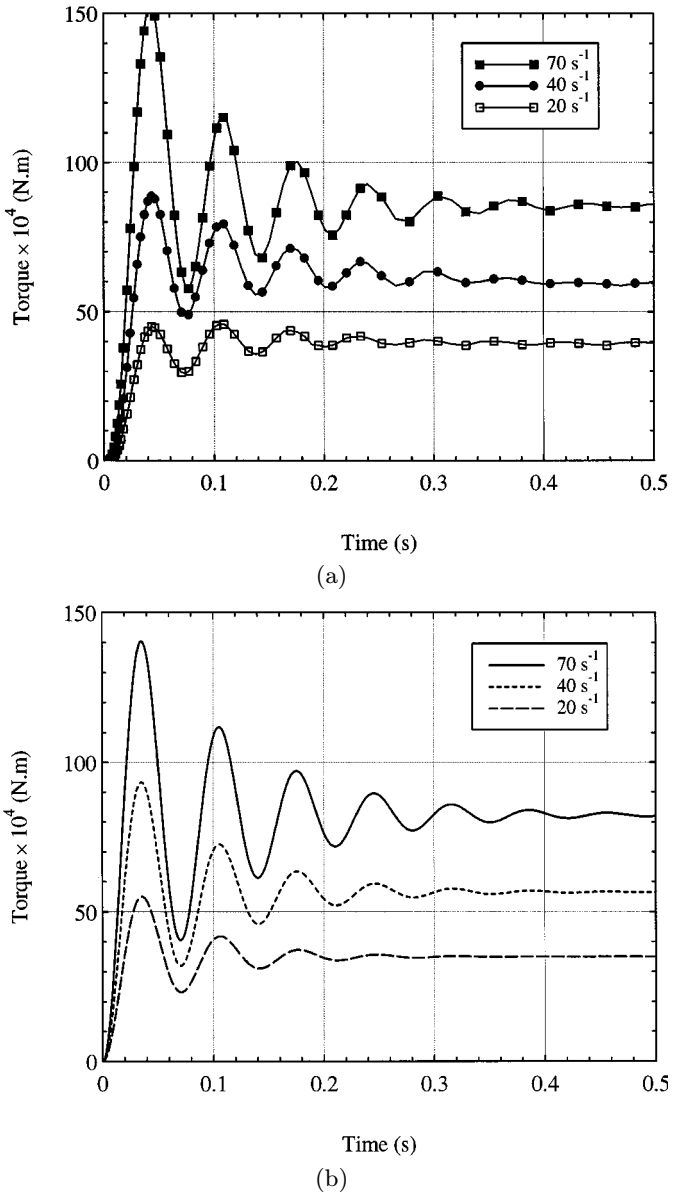

Fig. 17. The time evolution of the torque for the non-Newtonian fluid A (3 wt% CMC prolabo/97 wt% water). (a) experimental result; (b) code result.

parameters have been determined:

Fluid A	Fluid B
$\mu_r = 3.938$ Pa s	$\mu_r = 21.83$ Pa s
$\mu_\infty = 0.2011$ Pa s	$\mu_\infty = 0$ Pa s
$K = 0.1348$ s	$K = 0.3997$ s
$n = 0.54$	$n = 0.69$.

The standard error of fit is of 0.86 for fluid A and of 0.37 for fluid B. In comparison, the power law gives a standard error of 11.8 for fluid A and of 25.24 for fluid B.

These parameters have been used in the code "RHEOUTIL" to simulate step procedure in the Weissenberg device.

Figures 17a and 17b depict respectively, the experimental and simulated results obtained for fluid A at different rotation speeds. The agreement between experiment and theory is rather good, for the oscillations observed during the transient period (frequency and amplitude) as well as for the established flow. The values obtained at steady state differ by less than 10%, even for the worse case (20 s^{-1}). The most important discrepancy lies in the amplitude of the oscillations. It is interesting to note that the experimental amplitudes are larger than the calculated values for the highest rotation speed. The opposite can be observed for the lowest rotation speed. In this case, one can remark that the experimental amplitude of the second oscillation is almost as large as the first one. This is quite difficult to analyze in this case, but will be emphasized in the case of fluid B.

Figures 18a and 18b show respectively, the experimental and numerical results obtained with fluid B. Here, the two sets of curves are very different. For all experimental curves, one can observe that the first oscillation seems to be weakened, which is inconsistent with the numerical results. In addition, the pseudo steady state value becomes very different as the rotation speed increases: the difference, which is negligible for the lowest shear rate (2 s^{-1}) rises up to around 30% for the highest value (20 s^{-1}). The specific shape of the oscillating curves and the equilibrium values must be ascribed to time-dependent behaviour of that fluid.

The only tendency that we can find on both graphs is the non-linear effect of the velocity due to the shear-thinning fluid: the way the oscillations are damped out strongly depends on the rotation speed.

Concerning the lubrication assumption, the ratio τ/T given by equation (7.9) is calculated for all the cases presented previously (fluid A and fluid B). The values obtained by using the equilibrium value of the apparent viscosity remain less than 10^{-2}. Taking into account the result obtained in the first part, one knows that the time constant of the diffusion process is more important than the one calculated with the equilibrium value of the apparent viscosity. Nevertheless, these values of the ratio τ/T give a good range order and one can deduce that the fluid inertia is negligible and hence, the lubrication assumption remains valid. Because of the complexity of the constitutive model (Eq. (8.4)), equation (7.2) has been solved numerically. The results obtained with the lubrication assumption are in a good agreement with the results of the code "RHEOUTIL".

In conclusion, the discrepancy between experiment and simulation allows us to reveal rheological properties that are not taken into account in the constitutive model as determined by the flow procedure. This is an example of how such a numerical tool permits the transient period to be analyzed in order to improve the comprehension of fluid complexity.

8.2 Time dependent effects and prospects

The fluid B exhibits quite evident time dependent properties. The shape of the torque curve obtained for a shear

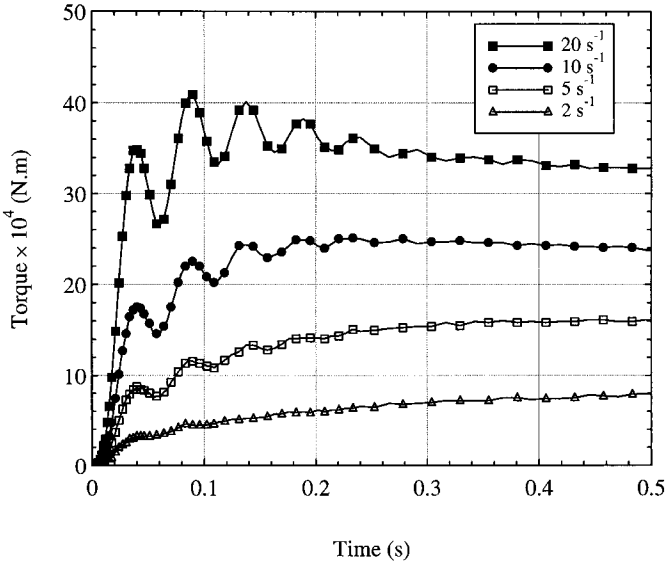

(a)

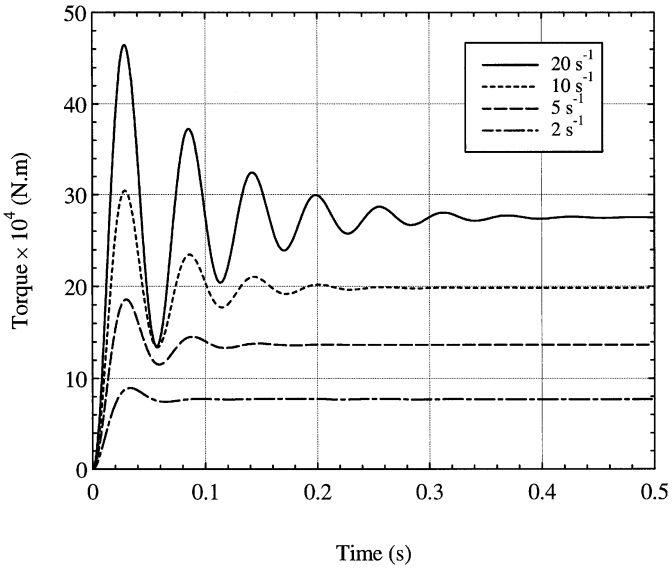

(b)

Fig. 18. The time evolution of the torque for the non-Newtonian fluid B (2 wt% CMC tylose/98 wt% water). (a) experimental result; (b) code result.

rate of 20 s^{-1}) can be interpreted in terms of structure breakdown of the fluid. However, it is more difficult to observe the effects of the viscoelastic properties of this material for that kind of test.

Figure 19 depicts the typical response of a thixotropic fluid supplied to a step test [34]. The fluid consists of a mixture of 3% of Veegum (clay), 1% of CMC and water ($\dot{\gamma}$ = 30 s^{-1}). Observing what happens during the first seconds reveals again the damped out oscillations. Keeping in mind that thixotropic fluids involve the concept of memory, it is necessary to know the whole history of the fluid, in particular at short times of the process. In addition, this time-dependent fluid exhibits also viscoelastic

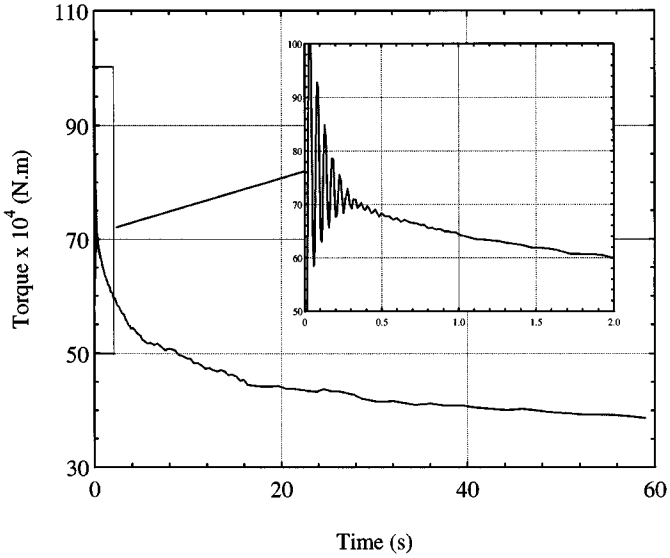

Fig. 19. The time evolution of the torque for a thixotropic fluid (3 wt% veegum, 1 wt% CMC, 96 wt% water).

and yield stress properties. Note that the yield stress depends on the structure of the fluid.

Now, the great challenge is to be able to characterize correctly that kind of complex fluid. One of the main idea proposed to achieve this aim is to use the flexibility provided by the numerical simulation. This flexibility allows to test more easily and hence to estimate the respective weight of the different rheological properties of the complex fluids. As a first step, one may consider that these different aspects of the fluid are not coupled. Then, it would be interesting to analyze the coupling effects, for instance, between thixotropic and viscoelastic properties, and thixotropic and yield stress properties. For a given experimental configuration, the more complicated are the rheological properties of the fluid, the more complicated is the fluid flow and the more difficult is the rheometrical results to be analyzed. In that case the numerical simulation can be an useful and essential tool.

However, it is clear that the numerical simulation will not be able to solve alone this whole problem. As we demonstrate in the second part of this paper, the experiment plays the most important part, by providing the backbone of the research work. Illustrating this important idea, the experimental results obtained for the fluid B and the thixotropic fluid show out that the code "RHEOUTIL" has to evolve again to take into account more complex aspects of fluid rheology.

9 Conclusion

The first part of this paper was devoted to the development of a numerical code able to account for the unsteady flow in the cone and plate geometry for different constitutive laws of purely viscous fluids. This part, devoted to a large audience, allows a better comprehension

of the rheometric limitations occurring when measuring the rheological properties of Newtonian or non Newtonian fluid.

In the second part, the possibilities offered by this numerical code have been highlighted by confronting the numerical results with experimental data obtained with the Weissenberg rheometer. In the first part we considered that the apparatus was perfect. Actually, the very bad agreement initially found between measurement and calculation, even with Newtonian fluids, was due to the disturbance induced by the torque measurement system of the apparatus. Indeed, during the transient period, the latter gives rise to a fluid structure interaction which changes dramatically the physical phenomena.

Keeping in mind that an apparatus can never be perfect, the strategy adopted here has been to take advantage of the flexibility procured by the numerical simulation to account for this particular device in the formulation of the boundary conditions. The new formulation allowed the agreement to be good. The present work shows how realistic physical assumptions coupled with an efficient numerical method can assist with the interpretation of experiment.

By assuming a steady state flow in the fluid sample, we proposed, for Newtonian fluids, an analytical solution in order to simulate the fluid structure interaction. This solution allowed us to propose a criterion able to know if it is possible to assume steady state. The conclusion is that this assumption is usually valid for most of the configurations encountered with the cone and plate geometry. Nevertheless, in some cases, slight differences can be observed between the analytical solution and the numerical calculation. All are due to the time diffusion of the momentum through the fluid sample.

The main advantage of the numerical simulation is obviously its possibility to deal with non Newtonian fluids, and especially with time dependent fluid.

Experimental results obtained for two different shearshinning fluids have been computed with the model, with parameters of the constitutive law determined during a flow protocol. The comparison between the experiment and the simulation is able to reveal certain failures in the choice of the constitutive equation. In particular, an initial breakdown of the structure can be deduced from this comparison.

The simplified version of the code is incapable to simulate the flow of that kind of fluid during unsteady state. Indeed, the code "RHEOUTIL" is only valid for purely viscous fluids and cannot take into account the elastic properties of fluid.

These results prove that the transient period is of fundamental importance in the case of time-dependent fluids. Only a numerical tool will allow us to exploit the transient period in order to improve the characterization of complex fluids. Future works will be devoted to the elaboration of a new code in order to characterize time dependent fluids as thixotropic and viscoelastic fluids.

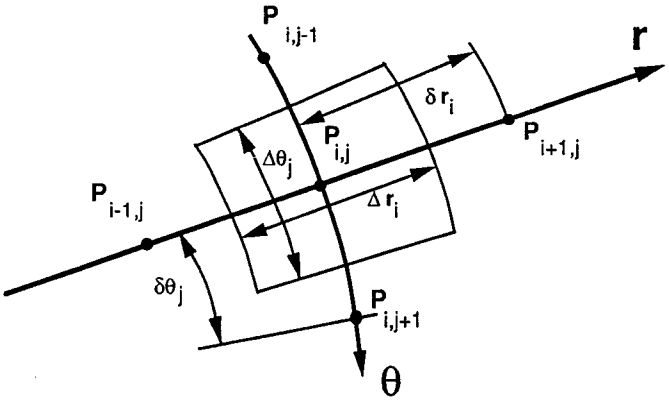

Fig. 20. Control-volume. For a non-uniform grid, the distance between two points and the volume width would be different.

Appendix A: Solving the problem

A.1 Presentation of the numerical method

The control volume formulation developed by Patankar [27] was adapted to the cone and plate geometry to determine the velocity field. The basic idea is to divide the continuum calculation domain into a number of non-overlapping control volumes. One control volume surrounds each grid point, where the unknown velocity has to be determined. The differential equation is integrated over each control volume in order to be discretised.

As explained in Patankar's book [27]: "*The most attractive feature of the control-volume formulation is that the resulting solution would imply that the integral conservation of momentum is exactly satisfied over any group of control volumes and, of course, over the whole calculation domain.*"

Figure 20 illustrates the characteristics of the volume V_{ij}, surrounding the grid point P_{ij} located at its center of gravity. The indices of the volume boundaries are $i-\frac{1}{2}$, j and $i+\frac{1}{2}$, j in the r direction i, $j+\frac{1}{2}$ and i, $j-\frac{1}{2}$ in the θ direction. It is a formal notation which is only exact when the grid is regular. If the equilibrium equation (3.4) is integrated over the control volume V_{ij} and over the time interval from t to $t+\Delta t$, one obtains:

$$\int_t^{t+\Delta t}\int_{V_{ij}}\left[\rho\frac{\partial \mathbf{U}}{\partial t}-\mathbf{div}(-p\mathbf{I}+\Im)\right]dv\,dt=0. \qquad (A.1)$$

Using the divergence theorem, equation (A.1) becomes:

$$\int_t^{t+\Delta t}\left[\int_{V_{ij}}\rho\frac{\partial \mathbf{U}}{\partial t}dv\,dt-\int_{\sum_{ij}}(-p\mathbf{I}+\Im)\mathbf{n}\,ds\right]dt=0. \qquad (A.2)$$

In the φ direction, equation (A.2) gives:

$$\rho V_{ij}\Big(U_\varphi(t+\Delta t)-U_\varphi(t)\Big) = \Big[\int_{\sum_{ij}}(-p\mathbf{I}+\Im)\cdot\mathbf{n}\,ds\Big]\cdot\mathbf{n}_\varphi\,\Delta t \qquad (A.3)$$

The assumptions necessary to obtain equation (A.3) are the followings: for the unsteady term, the grid-point value of U_φ is assumed to prevail throughout the control volume. In other respects, the integral over $\sum_{ij}$ is assumed to be constant during Δt and is determined at $t+\Delta t$. Such a scheme is fully implicit.

A.2 Balance over the control-volume

The stress fluxes in equation (A.3) are expressed over the different sides of the $\sum_{ij}$ boundary of the control volume. This volume being defined within a part of the space delimited by the infinitesimal angle $d\varphi$, the balance must be made over its six sides. Indeed, if there is no problem with sides having normal vectors $\mathbf{n}_r$ and $\mathbf{n}_\theta$, it is certainly not the case for the $\mathbf{n}_\varphi$ direction.

- Balance over the sides $(i-\frac{1}{2},\, j)$ and $(i+\frac{1}{2},\, j)$ (normal $\mathbf{n}_r$):

$$(r^2_{i+\frac{1}{2}} d\varphi \Delta\theta_j \sin\theta_j)(\tau_{r\varphi})_{i+\frac{1}{2}j} - (r^2_{i-\frac{1}{2}} d\varphi \Delta\theta_j \sin\theta_j)(\tau_{r\varphi})_{i-\frac{1}{2}j}. \quad \text{(A.4)}$$

- Balance over the sides $(i,\, j+\frac{1}{2})$ and $(i,\, j-\frac{1}{2})$ (normal $\mathbf{n}_\theta$):

$$(r_i\, \Delta r_i\, d\varphi\, \sin\theta_{j+\frac{1}{2}} (\tau_{\theta\varphi})_{(ij+\frac{1}{2})} - (r_i\, \Delta r_i\, d\varphi\, \sin\theta_{j-\frac{1}{2}})(\tau_{\theta\varphi})_{(ij-\frac{1}{2})}. \quad \text{(A.5)}$$

- Balance over the sides in $\mathbf{n}_{\varphi+\frac{1}{2}}$ and $\mathbf{n}_{\varphi-\frac{1}{2}}$ directions: Note that the vectors $\mathbf{n}_{\varphi+\frac{1}{2}}$ and $\mathbf{n}_{\varphi-\frac{1}{2}}$ being not exactly perpendicular to the vectors $\mathbf{n}_r$ and $\mathbf{n}_\theta$, the balance gives another term in the $\mathbf{n}_\varphi$ direction.

$$r_i\, \Delta r_i\, d\varphi\, \Delta\theta_j \Big(\sin\theta_j (\tau_{r\varphi})_{ij} + \cos\theta_j (\tau_{\theta\varphi})_{ij}\Big). \quad \text{(A.6)}$$

Equation (A.6) is obtained by considering the traction $\mathbf{F}_{\varphi+\frac{1}{2}}$ and the traction $\mathbf{F}_{\varphi-\frac{1}{2}}$. on sides with normal $\mathbf{n}_{\varphi+\frac{1}{2}}$ and $\mathbf{n}_{\varphi-\frac{1}{2}}$ respectively. When the angle φ varies by a quantity $d\varphi$, there is a variation of $\mathbf{n}_\varphi$which induces a variation of $\mathbf{n}_r$ and $\mathbf{n}_\theta$, the expression is given by:

$$d\mathbf{n}_r = \sin\theta \frac{d\varphi}{2} \mathbf{n}_\varphi \quad \text{and} \quad d\mathbf{n}_\theta = \cos\theta \frac{d\varphi}{2} \mathbf{n}_\varphi.$$

Therefore the traction $\mathbf{F}_{\varphi+\frac{1}{2}}$ and the traction $\mathbf{F}_{\varphi-\frac{1}{2}}$ are expressed as:

$$\mathbf{F}_{\varphi+\frac{1}{2}} = \tau_{r\varphi}\big(\mathbf{n}_r + \sin\theta \frac{d\varphi}{2}\mathbf{n}_\varphi\big) + \tau_{\theta\varphi}\big(\mathbf{n}_\theta + \cos\theta \frac{d\varphi}{2}\mathbf{n}_\varphi\big) \quad \text{(A.7)}$$

$$\mathbf{F}_{\varphi-\frac{1}{2}} = \tau_{r\varphi}\big(\mathbf{n}_r - \sin\theta \frac{d\varphi}{2}\mathbf{n}_\varphi\big) - \tau_{\theta\varphi}\big(\mathbf{n}_\theta - \cos\theta \frac{d\varphi}{2}\mathbf{n}_\varphi\big). \quad \text{(A.8)}$$

The balance over the two sides gives :

$$\mathbf{F}_{\varphi+\frac{1}{2}} + \mathbf{F}_{\varphi-\frac{1}{2}} = \tau_{r\varphi} \sin\theta d\varphi\, \mathbf{n}_\varphi + \tau_{\theta\varphi} \cos\theta d\varphi\, \mathbf{n}_\varphi. \quad \text{(A.9)}$$

Consequently, the discretised form of equation (3.7) is:

$$\begin{aligned}
&\rho\left(\frac{u^{n+1}_{ij} - u^n_{ij}}{\Delta t}\right) \\
&= \frac{r^2_{i+\frac{1}{2}}}{r_i^2 \Delta r_i}(\tau_{r\varphi})_{i+\frac{1}{2}j} - \frac{r^2_{i-\frac{1}{2}}}{r_i^2 \Delta r_i}(\tau_{r\varphi})_{i-\frac{1}{2}j} \\
&\quad + \frac{\sin\theta_{j+\frac{1}{2}}}{r_i \Delta\theta_j \sin\theta_j}(\tau_{\theta\varphi})_{ij+\frac{1}{2}} - \frac{\sin\theta_{j-\frac{1}{2}}}{r_i \Delta\theta_j \sin\theta_j}(\tau_{\theta\varphi})_{ij-\frac{1}{2}} \\
&\quad + \frac{(\tau_{r\varphi})_{ij}}{r_i} + \cot\theta_j \frac{(\tau_{\theta\varphi})_{ij}}{r_i}
\end{aligned} \quad \text{(A.10)}$$

where u^n and u^{n+1} represent the velocities at time t and $t+\Delta t$, respectively. Due to the choice of a full implicit scheme, the right hand side of equation (A.10) is evaluated at time $t+\Delta t$.

A.3 Discretised equations according to the behaviour model

Let us consider the constitutive equation (3.2) written as:

$$\Im = 2\mu(\mathcal{D}_{II})\mathcal{D} \quad \text{(A.11)}$$

where

$$\mathcal{D}_{II} = \frac{1}{2}[tr(\mathcal{D}^2)] \quad \text{(A.12)}$$

$$\mathcal{D}_{II} = (\dot\varepsilon^2_{r\varphi} + \dot\varepsilon^2_{\theta\varphi}) \quad \text{(A.13)}$$

$$\dot\varepsilon_{r\varphi} = \frac{1}{2}\left(\frac{\partial U_\varphi}{\partial r} - \frac{U_\varphi}{r}\right) \quad \text{(A.14)}$$

$$\dot\varepsilon_{\theta\varphi} = \frac{\partial U_\varphi}{\partial\theta} - \cot\theta U_\varphi). \quad \text{(A.15)}$$

Considering the constitutive equation and the tensor $\mathcal{D}$ expression, the discretised equation (A.10) becomes:

$$\begin{aligned}
&\rho\left(\frac{u^{n+1}_{ij} - u^n_{ij}}{\Delta t}\right) \\
&= \frac{r^2_{i+\frac{1}{2}}\mu_{i+\frac{1}{2}j}}{r_i^2 \Delta r_i}\Big(\frac{u_{i+1\,j} - u_{ij}}{\delta r_i} - \frac{u_{i+1\,j} + u_{ij}}{2r_{i+\frac{1}{2}}}\Big) \\
&\quad - \frac{r^2_{i-\frac{1}{2}}\mu_{i-\frac{1}{2}j}}{r_i^2 \Delta r_i}\Big(\frac{u_{ij} - u_{i-1\,j}}{\delta r_{i-1}} - \frac{u_{ij} + u_{i-1\,j}}{2r_{i-\frac{1}{2}}}\Big) \\
&\quad + \frac{\sin\theta_{j+\frac{1}{2}}\mu_{ij+\frac{1}{2}}}{r_i^2 \sin\theta_j \Delta\theta_j}\Big(\frac{u_{ij+1} - u_{ij}}{\delta\theta_j} - \frac{u_{ij+1} + u_{ij}}{2}\cot\theta_{j+\frac{1}{2}}\Big) \\
&\quad - \frac{\sin\theta_{j-\frac{1}{2}}\mu_{ij-\frac{1}{2}}}{r_i^2 \sin\theta_j \Delta\theta_j}\Big(\frac{u_{ij} - u_{ij-1}}{\delta\theta_{j-1}} - \frac{u_{ij} + u_{ij-1}}{2}\cot\theta_{j-\frac{1}{2}}\Big) \\
&\quad + \frac{\mu_{ij}}{r_i}\Big[\frac{1}{2}\Big(\frac{u_{i+1\,j} - u_{ij}}{\delta r_i} + \frac{u_{ij} - u_{i-1\,j}}{\delta r_{i-1}}\Big) - \frac{u_{ij}}{r_i}\Big] \\
&\quad + \frac{\mu_{ij}\cot\theta_j}{r_i^2}\Big[\frac{1}{2}\Big(\frac{u_{ij+1} + u_{ij}}{\delta\theta_j} + \frac{u_{ij} - u_{ij-1}}{\delta\theta_{j-1}}\Big) - \cot\theta_j u_{ij}\Big].
\end{aligned} \quad \text{(A.16)}$$

Note that μ is a function of $\mathcal{D}_{II}$ in the equation (A.16). From this equation, it is possible to recover the momentum equation written for a Newtonian fluid in spherical coordinates.

As suggested by Patankar [27], it is useful to write the above equation in the form:

$$Au_{ij} = Bu_{i+1\,j} + Cu_{i-1\,j} + Du_{ij+1} + Eu_{ij-1} + F. \tag{A.17}$$

The values of the subscripts appearing in the coefficients A, B, C, D, E and F are important when the grid is not regular or when the fluid is non Newtonian.

Assembling the equations for all grid points leads to a system of equations which is linear only when the fluid under test is Newtonian. Actually, since the problem is non-linear for complex fluids, it is better to solve several sub-systems of equations per iteration. The system has been solved by a Gauss-Seidel line method, see Hirsch [35]. After a complete sweep for both directions, all coefficients are calculated with the new field of estimated values. The convergence criterion uses the $||\ L\ ||_\infty$ norm. Basically, in order to solve the system, an iterative process is used because of the choice of the solving strategy (Gauss-Seidel line method) and because of the coefficients A, B, C, D, E which can be function of the unknown velocity field. In the first case, one talks about inner iterations and in the second one about outer iterations. As a final remark, it should be noted that the code controls automatically the time increment and under-relaxation factors.

Appendix B: Model validation: Use of analytical solutions for Newtonian fluid

B.1 Steady state flow

In this part, we investigate the agreement of the numerical results with an analytical solution proposed by Bird *et al.* [36]. The tested fluid is water.

In the case, a constant angular velocity is imposed on the rotor, the velocity field is:

$$U_\varphi = r\omega \sin\theta_0 \frac{\cot\theta + 0.5 \ln\left(\frac{1+\cos\theta}{1-\cos\theta}\right)\sin\theta}{\cot\theta_0 + 0.5 \ln\left(\frac{1+\cos\theta_0}{1-\cos\theta_0}\right)\sin\theta_0}\cdot \tag{B.1}$$

For θ and θ_0 approximately equal to $\pi/2$, this expression exhibits a linear relation between U_φ and ψ. This can be observed in Figures 2 and 4 near the steady state ($t^* = 0.73$).

However, a real test for the model is to compare the profiles for very large angles. We present here results obtained with $\psi_0 = 60°$. The velocity profiles at different radii give very good agreement between the analytical solution and the numerical results (Fig. 21). Note that these profiles can no longer be considered as linear functions of ψ when this angle is greater than 4°. Obviously, considering ψ_0 values and the nature of the fluid (water), this formal calculation cannot be interpreted on a practical point of view.

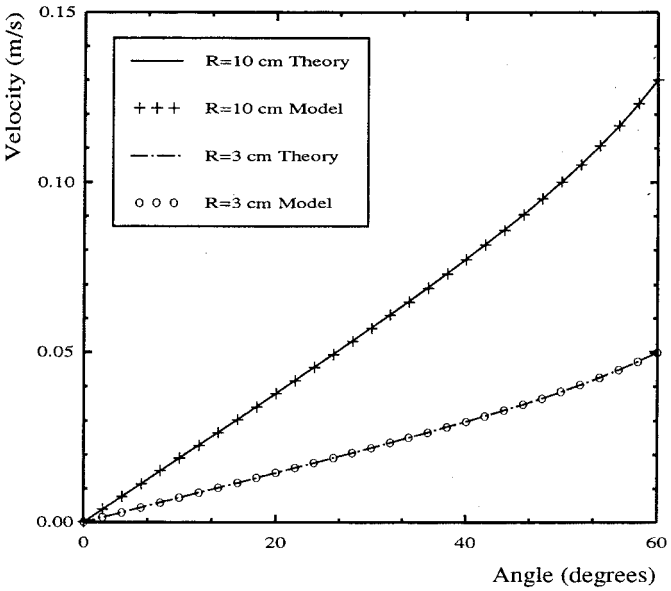

Fig. 21. Newtonian fluid ($\mu = 10^{-3}$ Pa s, $\rho = 10^3$ kg m^{-3}). Code validation for steady state flow ($\psi_0 = 60°$).

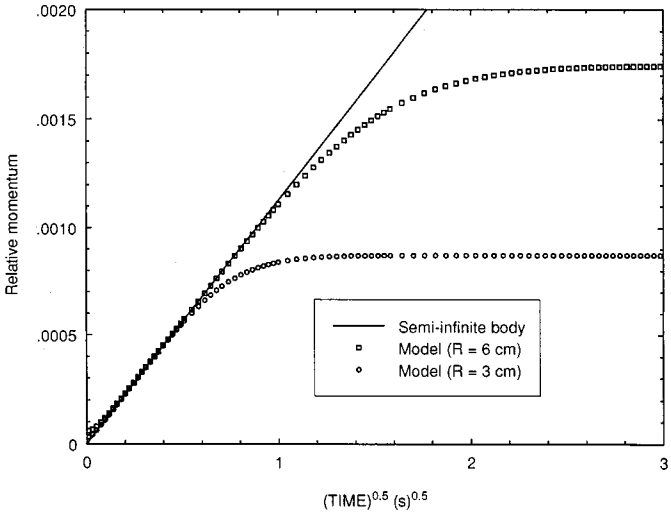

Fig. 22. Newtonian fluid ($\mu = 10^{-3}$ Pa s, $\rho = 10^3$ kg m^{-3}). Code validation for transient period.

B.2 Unsteady state flow

We have also checked the validity of our numerical results during the transient period. The idea is to analyze the numerical results for a step of the rotational speed. For short times, the phenomenon looks like diffusion from a plate at velocity $V = r\omega_0$ through a semi-infinite body. In this case, the fluid momentum is directly proportional to the square root of time:

$$Q = \int_0^{\psi_0} \rho\, U_\varphi\, r\, d\psi = \rho r \omega_0 \frac{2}{\sqrt{\pi}} \sqrt{\frac{\mu t}{\rho}}\cdot \tag{B.2}$$

The relative momentum ($Q/\rho r\omega_0$) calculated during test 1 for two different radii is in very good agreement with the expression (Eq. (B.2)). Note that the gap between

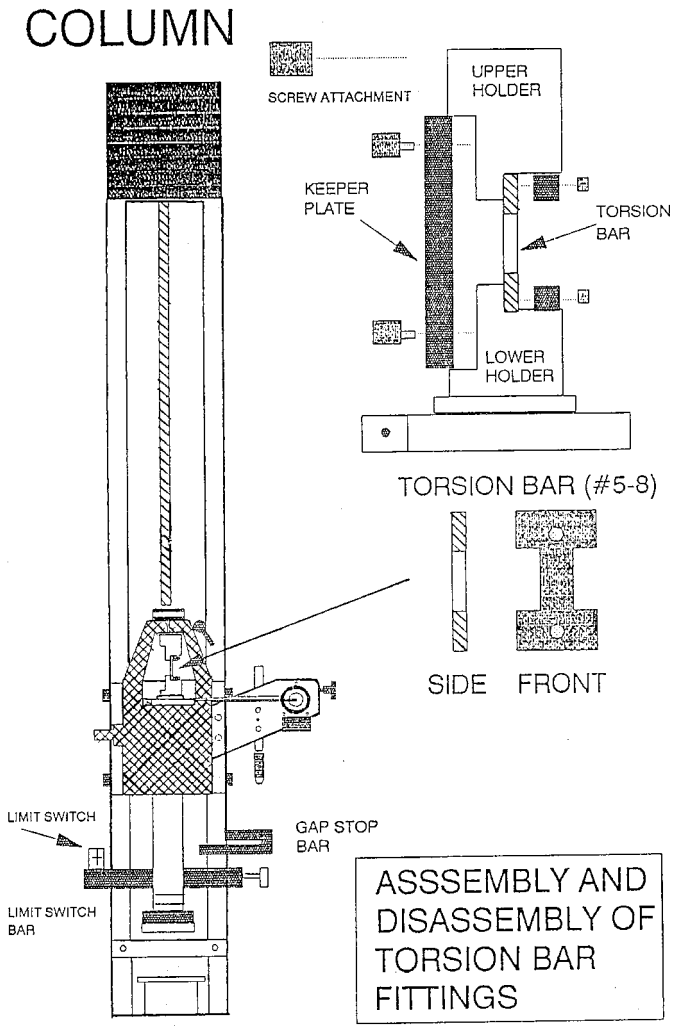

Fig. 23. Weissenberg rheometer.

the cone and the plate is finite and that the larger the radius, the wider the time interval of validity of this assumption (Fig. 22).

Appendix C: Description of the experiment

C.1 Equipment: The Weissenberg rheometer

Figure 23 shows the Weissenberg rheometer which is a controlled rotation speed device. However the real velocity of the rotor during the start up motion is not available. Indeed, the equilibrium value of the rotation speed is the single source of information, although the way of reaching this equilibrium is important during transient process. Nevertheless, if the time required to establish the rotor motion is very small compared with the diffusion time of the tested fluid, the rotor motion can be modeled by a step function. The high technology of the drive motor allows this assumption to be checked. Notice that the rotor and the stator represent the plate and the cone respectively.

The torsion bar forms the heart of the torque sensing system. Several torsion bars are available, all of them being I-shaped pieces of copper-bronze. They are cut so that the central stalk of the "I" is a different width for the various bar stiffness. The choice of the torsion bar depends on the range of the torque value. The larger the bar stiffness, the more torque required to achieve a given angular twist. The exact calibration value k of the torsion bar is included on a certificate for entry into the software. Measuring the torsion angle α allows the calculation of the twist torque $k\alpha$.

C.2 Test Characteristics

Firstly, the experimental results are obtained for three Newtonian fluids. Their calibrated values at 20 ℃ are respectively:

$$\mu_1 = 117 \text{ mPa s}, \qquad \rho_1 = 874 \text{ kg m}^{-3}$$
$$\mu_2 = 1929 \text{ mPa s}, \qquad \rho_2 = 908 \text{ kg m}^{-3}$$
$$\mu_3 = 13878 \text{ mPa s}, \qquad \rho_3 = 887 \text{ kg m}^{-3}.$$

The tests are carried out under the following conditions:

$$R = 3.75 \times 10^{-2} \text{ m} \qquad \psi = 2^\circ$$
$$k = 1.066 \text{ Nm rd}^{-1} \qquad I = 121.6 \times 10^{-6} \text{ Nm s}^2.$$

I characterizes the system inertia which is measured *via* the software by generating free oscillations of the system. In order to keep the same torsion bar, the shear rate used for each fluid must decrease as the viscosity increases. The following angular velocity values and corresponding mean shear rates have been used:

$$\omega_1 = 3.49 \text{ rd s}^{-1} \qquad (\dot{\gamma}_1 = 100 \text{ s}^{-1})$$
$$\omega_2 = 1.05 \text{ rd s}^{-1} \qquad (\dot{\gamma}_2 = 30 \text{ s}^{-1})$$
$$\omega_3 = 0.07 \text{ rd s}^{-1} \qquad (\dot{\gamma}_3 = 2 \text{ s}^{-1}.$$

In order to interpret physical phenomena, none of the signal treatments proposed by the apparatus was used. More information on the effect of such treatments can be found in the paper of Passard and Lebouché [37].

References

1. N.R. Kouitat, G. Maurice, M. Lucius, Cahiers Rhéol. **8**, 14 (1989).
2. N.R. Kouitat, G. Maurice, M. Lucius, Rheol. Acta **29**, 332 (1990).
3. M.M. Denn, K.C. Porteous, Chem. Eng. J. **2**, 280 (1971).
4. J.K. Okeson, A.H. Emery, Trans. Soc. Rheol. **19**, 81 (1975).

5. R.L. Crawley, W.W. Graessley, Trans. Soc. Rheol. **21**, 19 (1977).
6. S.R. Burdette, J. Non-Newtonian Fluid Mech. **32**, 269 (1989).
7. J.S. Lee, G.G. Fuller, J. Non-Newtonian Fluid Mech. **39**, 1 (1991).
8. N. Adams, A.S. Lodge, Phil. Trans. Roy. Soc. (London) **256**, 149 (1964).
9. D.C-H. Cheng, Brit. J. Appl. Phys. **17**, 353 (1966).
10. S. Oka, A. Takami, Jpn J. Appl. Phys. **16**, 258 (1967).
11. P. Chaturani, S. Narasimman, Acta Mech. **82**, 197 (1990).
12. D.B. Cox, Nature **193**, 670 (1962).
13. W.H. Hoppmann, C.E. Miller, Trans. Soc. Rheol. **7**, 181 (1963).
14. P.L. Bhatnagar, S.L. Rathna, Quart. J. Appl. Math. **16**, 329 (1963).
15. H. Giesekus, Rheol. Acta **6**, 339 (1967).
16. K. Walters, N.D. Waters, Polymer systems, **1**, 211 (Macmillan, London, 1968).
17. D.C-H. Cheng, Chem. Eng. Sci. **23**, 895 (1968).
18. R.M. Turian, Ind. Eng. Chem. Fundam. **11**, 361 (1972).
19. M.E. Fewell, J.D. Hellmus, Trans. Soc. Rheol. **21**, 535 (1977).
20. G. Heuser, E. Krause, Rheol. Acta **18**, 553 (1979).
21. T.H. Hou, Rheol. Acta **20**, 14 (1981).
22. D.O. Olagunju, L.P. Cook, J. Non-Newtonian Fluid Mech. **46**, 29 (1993).
23. D.O. Olagunju, J. Non-Newtonian Fluid Mech. **50**, 289 (1993).
24. D.F. Griffiths, K. Walters, J. Fluid Mech. **42**, 379 (1970).
25. D.J. Paddon, K. Walters, Rheol. Acta **18**, 565 (1979).
26. D.O. Olagunju, J. Rheol. **38**, 151 (1994).
27. S.V. Patankar, *Numerical heat transfer and fluid flow*, (Hemisphere, Washington DC, 1980).
28. P. Perre, A. Degiovanni, Int. J. Heat Mass Transfer, **33**, 2463 (1990).
29. G. Astarita, G. Marucci, *Principles of non Newtonian fluids mechanics*, (Mc Graw-Hill Book compagny, United Kingdom, 1974).
30. D.C-H. Cheng, Int. J. Cosm. Sci. **9**, 151 (1987).
31. L.B. Jackson, *Signals, Systems, and Transforms* (Addison-Wesley Publishing Company 1991).
32. G.K. Batchelor, *An introduction to fluid dynamics*, (Cambridge at the University Press, 1967).
33. Rheo Society, Weissenberg Rheogoniometer Notice.
34. J. Passard, M. Lebouché, Cahiers Rhéo. **13**, 20 (1994).
35. C. Hirsch, *Numerical computation of internal and external flows* (Wiley-Interscience Publication, **1**, 1990).
36. R.B. Bird, N.E. Steward, E.N. Lightfoot, *Transport phenomena*, (Wiley, New York, 1960).
37. J. Passard, M. Lebouché, Actes TIFAN **6**, 100 (1993).
38. K. Walters, *Rheometry: Industrial Applications* (Research Studies Press, Letchworth, 1980).